NEOPLASIA
www.neoplasia.com

Volume 15 Number 7 July 2013 pp. 694–711 694

Multimodal Microvascular Imaging Reveals that Selective Inhibition of Class I PI3K Is Sufficient to Induce an Antivascular Response[1,2]

Deepak Sampath*, Jason Oeh*,[3], Shelby K. Wyatt†,[3], Tim C. Cao†, Hartmut Koeppen‡, Jeffrey Eastham-Anderson‡, Liliane Robillard*, Calvin C. K. Ho†, Jed Ross†, Guanglei Zhuang§, Hani Bou Reslan†, Philip Vitorino¶, Kai H. Barck†, Sharon E. Ungersma†, Jean Michel Vernes#, Maresa Caunt¶, Nick Van Bruggen†, Weilan Ye¶, Ulka Vijapurkar*, Yu-Ju Gloria Meng#, Napoleone Ferrara§, Lori S. Friedman* and Richard A. D. Carano†

*Department of Translational Oncology, Genentech, Inc, South San Francisco, CA; †Department of Biomedical Imaging, Genentech, Inc, South San Francisco, CA; ‡Department of Research Pathology, Genentech, Inc, South San Francisco, CA; §Ferrara Lab, Genentech, Inc, South San Francisco, CA; ¶Department of Molecular Biology, Genentech, Inc, South San Francisco, CA; #Department of Biochemical and Cellular Pharmacology, Genentech, Inc, South San Francisco, CA

Abstract

The phosphatidylinositol 3-kinase (PI3K) pathway is a central mediator of vascular endothelial growth factor (VEGF)–driven angiogenesis. The discovery of small molecule inhibitors that selectively target PI3K or PI3K and mammalian target of rapamycin (mTOR) provides an opportunity to pharmacologically determine the contribution of these key signaling nodes in VEGF-A–driven tumor angiogenesis *in vivo*. This study used an array of microvascular imaging techniques to monitor the antivascular effects of selective class I PI3K, mTOR, or dual PI3K/mTOR inhibitors in colorectal and prostate cancer xenograft models. Micro-computed tomography (micro-CT) angiography, dynamic contrast-enhanced magnetic resonance imaging (DCE-MRI), vessel size index (VSI) MRI, and DCE ultrasound (DCE-U/S) were employed to quantitatively evaluate the vascular (structural and physiological) response to these inhibitors. GDC-0980, a dual PI3K/mTOR inhibitor, was found to reduce micro-CT angiography vascular density, while VSI MRI demonstrated a significant reduction in vessel density and an increase in mean vessel size, consistent with a loss of small functional vessels and a substantial antivascular response. DCE-MRI showed that GDC-0980 produces a strong functional response by decreasing the vascular permeability/perfusion-related

Abbreviations: DCE-MRI, dynamic contrast-enhanced magnetic resonance imaging; DCE-U/S, dynamic contrast-enhanced ultrasound; FMD, flow-mediated dilation; mTOR, mammalian target of rapamycin; micro-CT, micro-computed tomography; PI3K, phosphatidylinositol 3-kinase; VEGF-A, vascular endothelial growth factor A; VSI, vessel size index; S6RP, S6 ribosomal protein

Address all correspondence to: Richard A. D. Carano, PhD and Deepak Sampath, PhD, Genentech, Inc, 1 DNA Way, South San Francisco, CA 94080. E-mail: carano.richard@gene.com, sampath.deepak@gene.com

[1]Potential conflicts of interest are given as follows: All authors are or were employees of Genentech, a member of the Roche Group, and have/had financial holdings in Genentech/Roche during the course of this work. Genentech/Roche owns all patent rights.

[2]This article refers to supplementary material, which is designated by Figure W1 and is available online at www.neoplasia.com.

[3]These authors contributed equally to this work.

Received 13 February 2013; Revised 16 April 2013; Accepted 22 April 2013

DOI 10.1593/neo.13470

parameter, K^{trans}. Interestingly, comparable antivascular effects were observed for both GDC-980 and GNE-490 (a selective class I PI3K inhibitor). In addition, mTOR-selective inhibitors did not affect vascular density, suggesting that PI3K inhibition is sufficient to generate structural changes, characteristic of a robust antivascular response. This study supports the use of noninvasive microvascular imaging techniques (DCE-MRI, VSI MRI, DCE-U/S) as pharmacodynamic assays to quantitatively measure the activity of PI3K and dual PI3K/mTOR inhibitors *in vivo*.

Neoplasia (2013) 15, 694–711

Introduction

Angiogenesis is a hallmark of cancer where activation of proangiogenic factors predominates over antiangiogenic factors resulting in tumor vasculature growth [1]. Of these proangiogenic factors, vascular endothelial growth factor A (VEGF-A) has been identified as a central mediator of angiogenesis, promoting endothelial cell proliferation, survival, migration, and increased vascular permeability [2–5]. The approval of therapies that target VEGF-A or its receptors for the treatment of several types of solid tumors has provided clinical proof of concept that angiogenesis is an integral component of tumor cell growth and metastasis [6–8].

VEGF ligands bind to and activate three structurally similar type I receptor tyrosine kinases: VEGFR1/FLT1, VEGFR2/KDR, and VEGFR3/FLT4 [9,10]. VEGFR2 expression is restricted primarily to the vasculature and, upon ligand binding, mediates signal transduction primarily through the phosphatidylinositol 3-kinase (PI3K) pathway. The rate-limiting enzyme of this pathway is the lipid kinase, PI3K, and consists of enzymatic subunits that are subdivided, on the basis of sequence homology and substrate specificity, into class I, II, and III and the p85/p55 regulatory subunits [11]. The class I subgroup consists of p110α, p110β, p110δ, and p110γ isoforms that generate phosphatidylinositol 3,4,5-trisphosphate from phosphatidylinositol 4,5-bisphosphate, resulting in membrane anchorage of the effector kinases, Akt, and downstream activation of the mammalian target of rapamycin (mTOR) C1/C2 complexes [11]. Activating and transforming mutations in the *PIK3CA* gene of the p110α subunit of PI3K are commonly found in breast, colorectal, endometrial, and ovarian cancers [11–13]. Thus, there is a strong rationale for targeting PI3K in the context of both tumorigenesis and angiogenesis.

While PI3K inhibitors such as LY294002 and wortmannin have demonstrated antiangiogenic properties [14–17], the lack of selectivity and poor pharmaceutical properties of these drugs precludes assessment of the specific contribution of PI3K in regulating VEGF-mediated tumor angiogenesis *in vivo*. Moreover, the role of PI3K in angiogenesis has been primarily defined by using morphologic and histologic criteria during development [18]. The effects of a dual PI3K/mTOR selective inhibitor (BEZ-235) on tumor vascular physiology has been evaluated in a BN472 mammary carcinoma allograft model in which drug treatment altered physiological parameters associated with the tumor microvasculature leakage [19]. While this study also demonstrated decreased vascularization in normal tissue after BEZ-235 treatment, it did not address the direct effects of dual PI3K/mTOR inhibition on tumor vascular structure. The latter point is important because suppression of tumor vascular growth and decreased tumor vascularization are key structural changes consistent with effective antiangiogenic therapies [20–22]. Thus, collectively, the precise structural and functional consequences of selectively inhibiting the PI3K pathway on tumor angiogenesis have not been thoroughly documented. The advent of PI3K-selective small molecule inhibitors, as well as those that have dual PI3K and mTOR antagonistic activity, provides a unique opportunity to pharmacologically dissect the specific contribution of these key signaling nodes in VEGF-A–driven tumor angiogenesis. Moreover, the development of multiparametric imaging techniques enables investigators to quantitatively assess the activity of antiangiogenic drugs noninvasively *in vivo* using both structural and physiological end points [22–25].

In this study, an array of complimentary imaging techniques were employed to characterize the structural and functional changes induced in the tumor vasculature after treatment with class I PI3K (GNE-490 [26]), mTOR (rapamycin and GNE-861 [27]), and dual PI3K/mTOR (GDC-0980 [28–30]) inhibitors in highly vascularized colorectal (HM-7) cancer xenograft model that is sensitive to an anti–VEGF-A therapy [31]. In addition, a second, less vascularized, prostate (NCI-PC3) cancer xenograft model was also evaluated. The techniques include micro-computed tomography (micro-CT) angiography and vessel size index magnetic resonance imaging (VSI MRI) to assess vascular structure and dynamic contrast-enhanced MRI (DCE-MRI) and DCE ultrasound (DCE-U/S) to provide both functional and structural assessments of the tumor vasculature. Micro-CT angiography is an *ex vivo* technique that provides high-resolution three-dimensional (3D) images to assess tumor vascular structure as a means to quantify vascular density [22,24]. VSI MRI combined with ultrasmall superparamagnetic iron oxide (USPIO) nanoparticles provides robust measures of tumor microvascular structure [25,32,33]. The long half-life and minimal leakage of USPIOs increase the available time for imaging, yielding high signal-to-noise images to produce quantitative estimates of mean vessel size, blood volume (BV), and a vessel density–related parameter, Q [25,32,33]. DCE-MRI employs rapid imaging to assess the pharmacokinetics of a small molecule Gd-based contrast agent as the agent moves between the tumor vasculature and the interstitial space [34]. The time-series imaging data are fitted to a kinetic model that provides quantitative parameters associated with fractional plasma volume (v_p), extravascular extracellular leakage space (v_e), and the leakage rate, K^{trans}, a parameter sensitive to changes in both blood flow and permeability [23,34,35]. DCE-U/S imaging employs microbubble contrast agents to assess blood flow [36]. The microbubble contrast agents remain intravascular because of their size (1 to 3 μm) removing the need to account for leakage in blood flow estimates [36]. The focus of this study was to employ these pharmacological agents and techniques to address the following questions: 1) Does dual PI3K/mTOR

inhibition produce a strong and rapid antivascular (structural) response in tumors similar to other molecules (anti–VEGF-A) that interfere with VEGF's actions? 2) Is PI3K inhibition alone sufficient to generate this antivascular effect?

Given that potent and selective PI3K and dual PI3K/mTOR inhibitors have entered clinical development for the treatment of cancer [37], an additional goal of our study was to assess the utility of microvascular imaging end points as biomarkers to measure response to drug treatment *in vivo*. Assays currently employed in the clinic to measure the activity of PI3K pathway inhibitors in tumors assess change of pathway biomarkers in tumor biopsy sections by immunohistochemistry (IHC) or, recently, by suppression of glucose uptake *in vivo* by [^{18}F]-fluorodeoxyglucose positron emission tomography (FDG-PET) imaging [38]. However, both methodologies have limitations: 1) tumor biopsy collection is invasive and immunohistochemical evaluation is semiquantitative and 2) interpretation of FDG-PET results are confounded by hyperglycemia that is commonly associated with PI3K inhibitor treatment [39]. Given the essential role of PI3K in VEGF-mediated signal transduction during tumor angiogenesis, our aim was to determine the utility of the microvascular imaging techniques described above as pharmacodynamic assays to measure the activity of PI3K, mTOR, and dual PI3K/mTOR inhibitors *in vivo*.

Our preclinical data demonstrate that dual PI3K/mTOR inhibition produces a rapid and robust antivascular response, altering both tumor vascular structure and function. Interestingly, PI3K inhibition by GNE-490 generated similar antivascular responses (structural and physiological) to GDC-0980 suggesting that PI3K pathway inhibition at the level of PI3K itself is sufficient to generate antiangiogenic effects. In addition, our work demonstrates the utility of advanced noninvasive microvascular imaging techniques (DCE-MRI, VSI MRI, and DCE-U/S) to assess the pharmacodynamic activity of PI3K and dual PI3K/mTOR inhibitors *in vivo*.

Materials and Methods

Cell Lines and Inhibitors

HM-7 colorectal cancer cells were purchased from ATCC (Rockville, MD), and NCI-PC3 prostate cancer cells were obtained through a material transfer agreement between Genentech (South San Francisco, CA) and the National Cancer Institute (Fredrick, MD). Tumor cell lines were grown in RPMI 1640 media supplemented with 10% FBS, L-glutamine, and penicillin/streptomycin (Sigma-Aldrich, St Louis, MO) before implantation in immunocompromised mice. Human umbilical vein endothelial cells (HUVECs) were cultured in EGM-2 containing growth factor media (Lonza, Allendale, NJ). B20.4.1.1, GDC-0980, and GNE-490 were generated at Genentech.

Western Blot Analysis

HUVECs were starved for 16 hours before stimulation with EGM-2 containing growth factor media (Lonza) for 1 hour with DMSO (vehicle), 0.40 μM GNE-490, or 0.40 μM GDC-0980. Following treatment, cells were lysed and equal amounts of protein were separated by electrophoresis, transferred onto polyvinylidene difluoride (PVDF) membranes, and probed with monospecific primary antibodies (Cell Signaling Technology, Beverly, MA) to phosphorylated Akt (pAkt; S^{473} and T^{308}), total Akt (tAkt), phosphorylated S6 ribosomal protein (pS6RP; $S^{235/236}$), total S6RP (tS6RP), phosphorylated 4EBP ($T^{37/46}$), total 4EBP, phosphorylated eNOS, total eNOS, and β-actin. Primary binding was detected with LI-COR's IRDye 680 or IRDye 800 infrared secondary antibodies using the LI-COR Odyssey Imaging System.

Endothelial Cell Migration and Sprouting Assays

Real-time monitoring of endothelial cell migration was performed using the xCELLigence System and CIM-Plate 16 (Roche, Pleasanton, CA). The upper chamber was coated with 20 μg/ml fibronectin and seeded with 50,000 HUVECs in EBM-2 basal media followed by stimulation with EGM-2 endothelial growth factors in the presence or absence of 0.40 μM GNE-490 or 0.40 μM GDC-0980. Cells migrating into the bottom chamber in response to attractants contacted and adhered to the electronic sensors, resulting in an increase in impedance. The cell migration index values reflecting impedance changes were automatically recorded every 15 minutes. Angiogenic sprouting assays were performed using 20 μg/ml anti-ragweed IgG (control), 20 μg/ml bevacizumab (anti–VEGF-A), 0.40 μM GNE-490, or 0.40 μM GDC-0980 as previously described [40] but with conditioned media from fibroblasts. Cells were imaged using Molecular Devices (Sunnyvale, CA) ImageXpress Micro automated microscope with a 4× S Fluor objective and quantified with a modified neurite detection script (MetaXpress software; Molecular Devices).

Nuclear ELISA Apoptosis Assay

HUVECs were cultured in 96-well plates (5000 cells/well) in the presence of EGM-2 growth factor containing media and treated with 0.40 μM GNE-490, 0.40 μM GDC-0980, or DMSO vehicle for 48 hours. Cells were stained with Alamar blue for 2 hours before lysis, and apoptosis was determined (on the basis of the presence of cytoplasmic histone-associated DNA fragments) using the Cell Death Detection ELISA^{plus} Kit (Roche Applied Science, Indianapolis, IN).

Animal Models for In Vivo *Efficacy and Imaging*

All *in vivo* studies were approved by Genentech's Institutional Animal Care and Use Committee and adhere to the National Institutes of Health Guidelines for the Care and Use of Laboratory Animals. Human tumor xenografts for *in vivo* efficacy and imaging studies were established by subcutaneous injection of 3.5×10^6 HM-7 cells/nude mouse (Harlan Laboratories, Livermore, CA) or 5×10^6 NCI-PC3 cells/nude mouse (Charles River Laboratories, Hollister, CA). Animals were distributed into treatment groups when tumors reached a mean volume of approximately 150 to 250 mm^3. B20.4.1.1 (10 mg/kg) and rapamycin (6 mg/kg) were administered intraperitoneally (i.p.) in saline, while GDC-0980 (7.5 or 10 mg/kg), GNE-490 (30 mg/kg), and GNE-861 (100 mg/kg) were administered by oral gavage (p.o.) in 0.5% methycellulose/0.2% Tween 80 (MCT) vehicle over a treatment period spanning 7 days. For efficacy studies, drugs were administered at tolerated doses (based on <15% body weight loss) to tumor-bearing mice (n = 8–10/group) daily for 7 days. Body weights and tumor volumes [caliper-based ellipsoid model: $L \times W^2/2$, where the larger (L) and smaller (W) perpendicular dimensions are measured] were recorded twice weekly. Percent tumor growth inhibition (TGI) was calculated at the end of drug treatment on day 7 using the following formula: %TGI = 100 × (mean tumor volume in the vehicle-treated group at day 7 – mean tumor volume of drug-treated group at day 7/mean tumor volume of vehicle-treated group at day 7).

VEGF-A ELISA Assays

HM-7 tumor–bearing mice (n = 4/group) were treated with a single oral dose of MCT vehicle, GNE-490 (30 mg/kg), or GDC-0980 (10 mg/kg). Tumors from each group were harvested 1, 4, 8, and 24 hours post-dose, immediately frozen in liquid nitrogen, and homogenized for analysis of VEGF-A isoforms 121 and 165 as previously described [41].

PI3K Pathway Biomarker Assays

HM-7 or NCI-PC3 tumor xenograft fragments (n = 3–4/group) were collected following a single dose of drug or after 7 continuous daily doses. Tumors were dissected and immediately frozen in liquid nitrogen for biochemical analysis or fixed in 10% neutral buffered formalin for 24 hours and embedded in paraffin for IHC. Meso Scale Discovery (Rockville, MD) assays were performed as per the manufacturer's instructions for $pAkt^{S473}$, tAkt, $pS6RP^{S235/236}$, and tS6RP using 2 mg/ml protein lysates per well. Each sample was run in duplicate, analyzed on a SECTOR Imager 6000, and reported as a ratio of phosphorylated protein to total protein ± SEM.

Immunohistochemistry

Mouse endothelium marker, MECA-32, was evaluated using 5-μm paraffin sections of formalin-fixed tumor tissue, treatment with antigen retrieval buffer (VMSI, Oro Valley, AZ), and incubation with anti–MECA-32 (Cell Signaling Technology, Danvers, MA) at 37°C. Bound antibody was detected using DABMap technology (VMSI) and sections were counterstained with hematoxylin. Images were acquired by the Olympus (Center Valley, PA) Nanozoomer automated slide scanning platform (Hamamatsu, Hamamatsu City, Japan) at ×200 final magnification and analyzed in the Matlab software package (Mathworks, Natick, MA). Viable tumor regions were identified on the basis of the size, shape, and density of hematoxylin staining of individual viable tumor cells. The brown MECA-32 staining was isolated using a support vector machine trained to perform morphologic segmentation of individual vessels. The vascular fraction (%) = 100 × vascular area/viable tumor area was calculated.

Micro-CT Angiography

Micro-CT angiography studies were performed 24 hours (HM-7 model; n = 8–10/group) or 48 hours (NCI-PC3 model; n = 8–10/group) after a single dose of MCT (vehicle control) or drug at the doses and routes described above. Upon sacrifice, mice were perfused with lead chromate latex (MICROFIL; Flowtech, Carver, MA) under a state of pharmacologic vasodilation by sodium nitroprusside as previously described [24]. *Ex vivo* tumors were imaged on a SCANCO Medical (Brüttisellen, Switzerland) Micro-CT 40 System (45 kV, 177 μA, 450 milliseconds, and 16-μm isotropic voxels). The vascular network and tumor volume were automatically extracted from the images [24]. Vascular density was defined as the ratio of vascular volume to tumor volume [22,24].

Multispectral VSI MRI

Multispectral VSI MRI was performed pre-treatment and 24 hours post-treatment with 10 mg/kg GDC-0980 (n = 9) or vehicle control (n = 9) in HM-7 tumor xenografts on a 4.7-T Agilent (Santa Clara, CA) Unity Inova MRI System with an Agilent 20-mm two-loop surface coil. Eight coronal, 1-mm-thick slices were acquired with a 25.6 × 25.6 mm field-of-view (FOV) and 64 × 64 (diffusion and T_2 sequences) or 128 × 128 (T_2* sequence) matrix. A diffusion-weighted fast spin-echo multislice imaging sequence was used to obtain apparent diffusion coefficient (ADC) measurements: six b values (82–1129 s/mm^2), repetition time (TR) = 3 seconds, echo train length = 4, number of excitations (NEX) = 2, diffusion gradient length = 3.3 milliseconds, and diffusion gradient separation = 30 milliseconds. T_2 and M_0 maps were generated using a multiecho, multislice spin-echo imaging sequence [echo time (TE) = 5, 26, 47, 68 milliseconds, TR = 3 seconds, and NEX = 1]. T_2* maps were generated using a multiecho, multislice gradient echo sequence (TE = 5, 10, 15, 20, 25, 30, 35, 40 milliseconds, TR = 345 milliseconds, and NEX = 4). Subsequently, a USPIO contrast agent (200 μmol/kg, Molday ION; BioPAL Inc, Worcester, MA) was delivered through tail vein catheter, and post-contrast multiecho, multislice and multiecho, multislice gradient echo sequences were repeated to calculate T_2 and T_2* maps, respectively. Multispectral VSI MRI parameters (vessel density–related Q, VSI, and fractional BV) were calculated voxel by voxel in the viable tumor using a multispectral approach. The multispectral approach was similar to that described in Ungersma et al. [25] but differed in that only ADC and proton density features were employed in the K-means clustering and the tumor was classified into three classes (viable tumor, necrosis, and subcutaneous fat). Viable tumor volume and percent necrosis (ratio of the volume of necrosis class to the sum of the volumes of the viable and necrosis classes) estimates were calculated from the classification. Negative ΔR2 or ΔR2* values were assumed to result from poor perfusion; in these cases, Q and/or BV were set to zero and included in the mean estimates. However, only nonzero and positive values were assumed to be valid and were included in the VSI estimates.

Multispectral DCE-MRI

Multispectral DCE-MRI studies were performed in HM-7 tumor xenografts to compare 1) GDC-0980 (7.5 mg/kg, n = 9) and vehicle control (n = 11) pre-treatment, 4 and 24 hours post-treatment and 2) GDC-0980 (10 mg/kg, n = 13), GNE-490 (30 mg/kg, n = 11), and vehicle control (n = 14) pre-treatment and 24 hours post-treatment. MRI was performed with an Agilent 9.4-T MRI System employing an Agilent volume transmit (63 mm)/surface receive (20 mm) coil setup. Twelve coronal, 1-mm-thick slices were acquired with a 25.6 × 25.6 mm FOV and 64 × 64 matrix for ADC and T_2 mapping. ADC, T_2, and M_0 maps were acquired as described for VSI MRI with the exception of TR = 3.7 seconds for the diffusion-weighted fast spin-echo multislice imaging sequence. In both studies, pre-contrast 3D gradient echo data sets were acquired at 2° and 10° flip angles, TR = 6 milliseconds, and NEX = 4. The first study used TE = 1.81 milliseconds, FOV = 51.2 × 25.6 × 32 mm, and a 128 × 64 × 32 matrix, while the second study used TE = 1.26 milliseconds, FOV = 25.6 × 25.6 × 16 mm, and a 64 × 64 × 16 matrix. Gadodiamide (Omniscan; GE Healthcare, Little Chalfont, United Kingdom) at 1 mmol/kg in 100 μl was injected through a tail vein catheter following collection of the pre-contrast images. Post-contrast 3D gradient echo images were then acquired for 30 minutes using a 10° flip angle, TR = 6 milliseconds, NEX = 1, and TE = 1.81 milliseconds (first study) or 1.26 milliseconds (second study) approximately every 15 seconds (first study) or 9 seconds (second study). The DCE-MRI analysis of K^{trans}, v_p, and v_e was restricted to the viable tumor using a multispectral approach [23]. The volume of viable tumor and percent necrosis are estimated as previously described [42].

DCE-U/S Microbubble Reflow Kinetics

DCE-U/S studies were performed pre-treatment and 24 hours post-treatment in HM-7 tumor xenografts to compare 1) GDC-0980 (7.5 mg/kg, n = 6) and MCT (vehicle control, n = 6) and 2) GDC-0980 (10 mg/kg, n = 8), GNE-490 (30 mg/kg, n = 7), and MCT (vehicle control, n = 8). A Siemens Acuson Sequoia C512 System (Siemens Medical Solutions USA, Malvern, PA) equipped with a 15L8-S linear transducer was used for harmonic ultrasound imaging: frequency = 14 MHz, transmitted power = −10 dB/0.21 mechanical index, and 20 frames/s. A vascular microbubble contrast agent (DEFINITY; Lantheus Medical Imaging, North Billerica, MA) was delivered through a jugular vein catheter at a constant of 3 μl/min using a syringe pump. Following bubble destruction from a high-intensity pulse, reflow kinetics was fitted to a kinetic model [36]. Enhancement factor was defined as the percentage of voxels within the tumor area where the voxel's mean pre-contrast signal intensity was two SDs below the mean of the last 10 temporal samples.

Flow-mediated Dilation Reactive Hyperemia by Ultrasound

Flow-mediated dilation (FMD) reactive hyperemia studies were performed in C57/BL6 immunocompetent mice (Charles River Laboratories). Vascular function was determined by ultrasound examination of the femoral artery (FA) to FMD and nitroglycerin (NTG) dilatation. A study was performed to compare GDC-0980 (10 mg/kg, n = 9), GNE-490 (30 mg/kg, n = 9), and vehicle control (n = 9) 4 hours post-treatment. Hair from the ventral surface of the hind limbs was removed using Nair (Church & Dwight Co, Princeton, NJ) to enable b-mode imaging using the VisualSonics (Toronto, CN) Vevo770 with a 55-MHz imaging probe. For FMD, a baseline image of the FA was collected and a rubber band was subsequently used as a temporary tourniquet to occlude FA blood flow for 4 minutes. The rubber band was then released for reflow of the FA and an image was acquired every minute for 4 minutes and analyzed to estimate FA maximum diameter using manufacturer-supplied software tools. For NTG, a baseline image of the FA was collected, an i.p. injection of 20 μg of NTG was administered, and images were acquired every minute for 4 minutes and analyzed for FA maximum diameter.

Statistical Analysis

Statistical significance was defined as $P < .05$. To compare two groups, an unpaired t test assuming unequal variances was used; for three or more groups, a comparison with control using Dunnett's method was used. To compare pre-treatment to post-treatment data within a group, a matched paired t test was used. All summary statistics of the results are given as means ± SEM.

Results

Dual PI3K/mTOR Inhibition Induces Antivascular Effects and Results in Significant Loss of Functional Vessels

To determine the vascular response when both PI3K and mTOR are simultaneously blocked, the effects of a dual PI3K/mTORC1/C2 inhibitor, GDC-0980, on tumor vascular structure was initially evaluated in the HM-7 human colorectal cancer xenograft model since it is highly vascularized and sensitive to antiangiogenic agents such as a neutralizing antibody to rodent and human VEGF-A (B20.4.1.1) *in vivo* [31]. Daily oral administration of GDC-0980 at a maximum tolerated dose of 10 mg/kg was efficacious in the HM-7 xenograft model and resulted in 75% TGI (tumor volume at end of treatment, control: 882.35 ± 107.27 mm^3; GDC-0980: 215.31 ± 21.19 mm^3, $P < .001$; Figure 1*A*). Moreover, GDC-0980 was significantly more efficacious than B20.4.1.1 (B20.4.1.1: 447.55 ± 49.61 mm^3, $P < .01$;

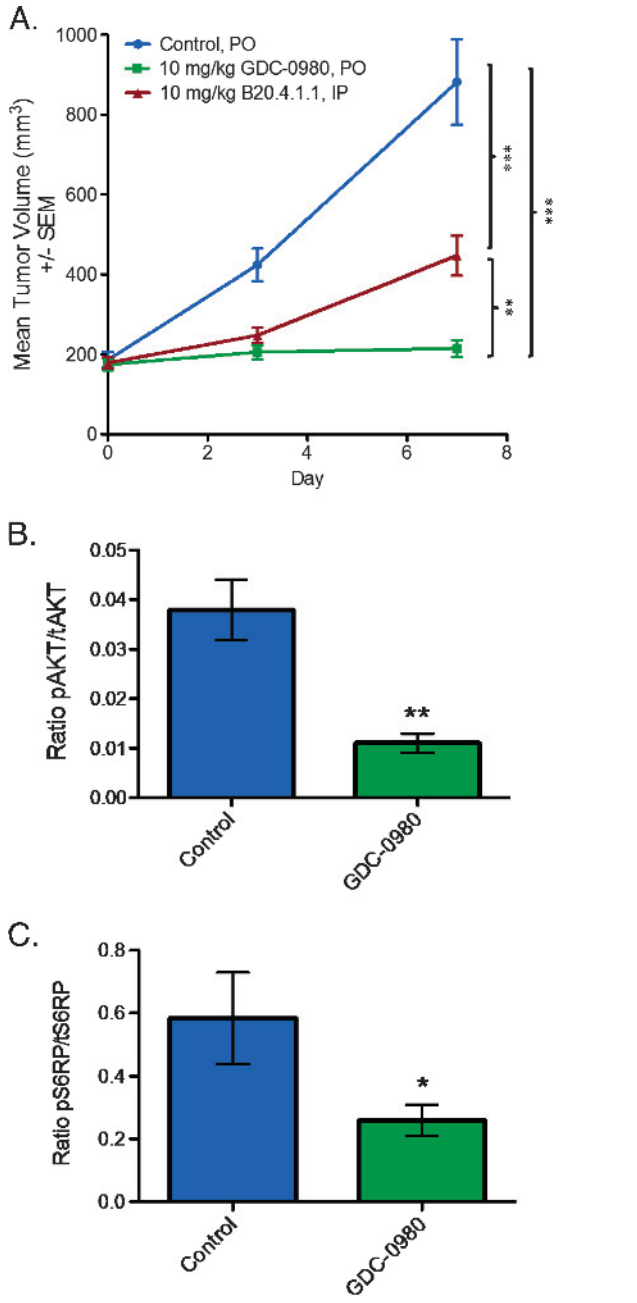

Figure 1. GDC-0980 is efficacious in the HM-7 colorectal cancer xenograft model. (A) Mean tumor volumes from HM-7 tumor–bearing mice (n = 8) treated daily and p.o. with MCT vehicle (control) or GDC-0980 (10 mg/kg) for 7 days. B20.4.1.1 (10 mg/kg) was administered i.p. on days 1 and 7. Comparisons to control were performed using Dunnett's method; comparisons between treatment groups were performed using unpaired t test assuming unequal variances: $^{**}P < .01$, $^{***}P < .001$. (B and C) HM-7 tumor–bearing mice (n = 4) were treated with a single oral dose of GDC-0980 (10 mg/kg) and harvested 1 hour post-dose to measure the levels of pAkt (S^{473}) normalized to tAkt (B) or pS6RP ($S^{235/236}$) normalized to tS6RP (C). $^{*}P < .05$, $^{**}P < .01$ compared to control using unpaired t test assuming unequal variances.

Figure 1*A*). Additionally, GDC-0980 treatment reduced the levels of PI3K and mTORC1/C2 proximal biomarkers, pAkt and pS6RP, respectively. Tumor pAkt levels were reduced by 71% (control: 0.028 ± 0.005; GDC-0980: 0.008 ± 0.002, $P < .01$) and pS6RP levels were reduced by 55% (control: 0.58 ± 0.15; GDC-0980: 0.26 ± 0.05, $P < .05$; Figure 1, *B* and *C*).

To assess the antivascular effects of GDC-0980, *ex vivo* micro-CT angiography was used to assess structural changes in the vasculature of HM-7 tumors with B20.4.1.1 employed as a positive control. Compared to control, both GDC-0980 and B20.4.1.1 significantly reduced vascular density relative to control (100 × vascular volume/tumor volume, control: 5.6 ± 0.4%; GDC-0980: 2.6 ± 0.2%, $P < .001$; B20.4.1.1: 3.8 ± 0.5%, $P < .01$; Figure 2, *A* and *B*), where the GDC-0980 group was also significantly reduced relative to the B20.4.1.1 group ($P < .05$). Assessment of the vascular endothelial marker, MECA-32, by IHC confirmed a significant reduction in the vascular area fraction (VAF = vascular area/viable tumor area) for both B20.4.1.1 and GDC-0980 treatments, with B20.4.1.1 also reduced relative to GDC-0980 (100 × VAF, control: 4.22 ± 0.36%; B20.4.1.1: 1.79 ± 0.16%, $P < .001$; GDC-0980: 3.22 ± 0.26%, $P < .05$; Figure 2, *C* and *D*). Histologically, the presence of small clusters of MECA-32–positive endothelial cells appears to have increased the vascular area estimate for the GDC-0980–treated groups since these vessels were not readily visible in the control or B20.4.1.1 groups (Figure 2*C*). These small MECA-32–positive cell clusters may represent remnants of collapsed vessels as a result of an antivascular response to GDC-0980 and may have been undetected by micro-CT angiography due to a lack of patency.

To specifically address whether a loss of patency contributed to the antivascular response by GDC-0980, *in vivo* multispectral VSI MRI

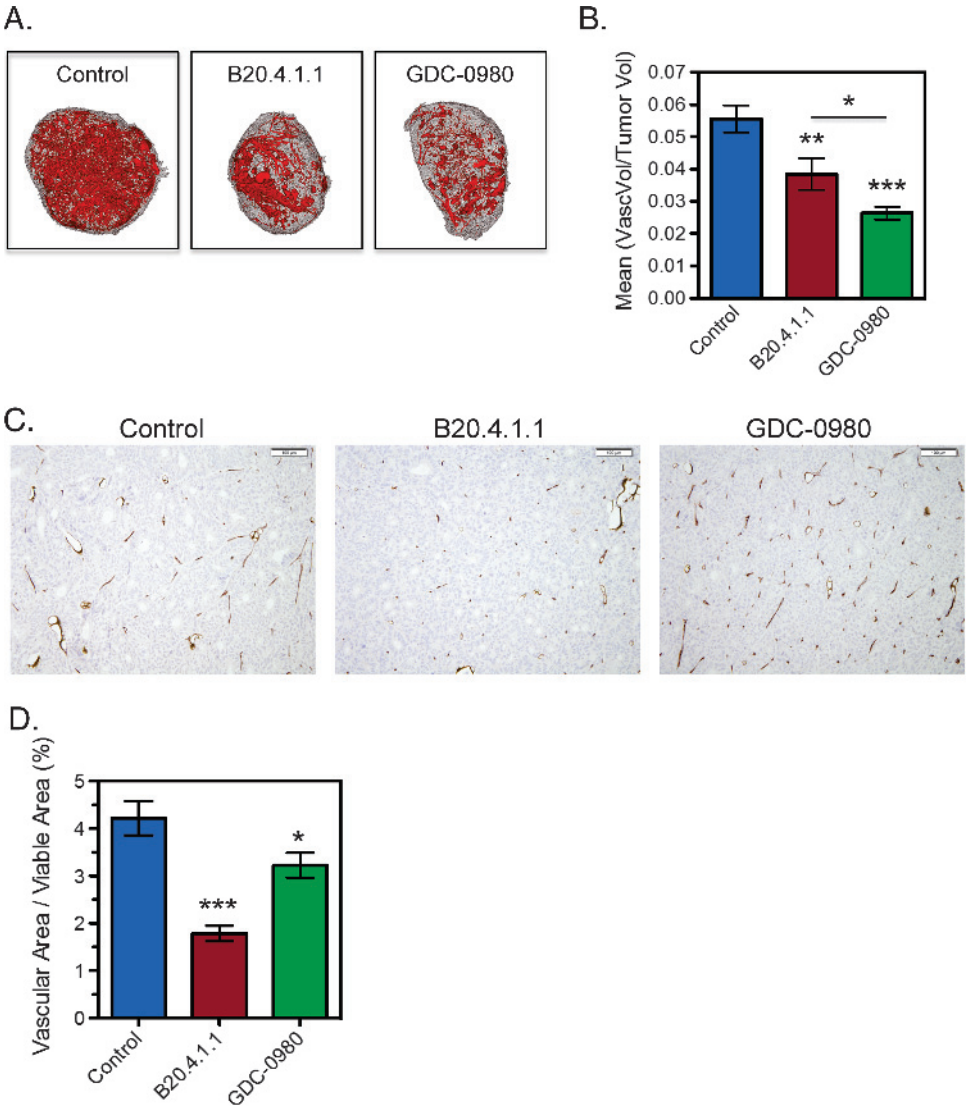

Figure 2. GDC-0980 reduces vascular density in the HM-7 colorectal cancer xenograft model. (A) Representative 3D renderings of the micro-CT–derived vascular skeleton (red) overlaid onto the tumor tissue (gray) 24 hours following a single dose of MCT vehicle (control), B20.4.1.1 (10 mg/kg), or GDC-0980 (10 mg/kg). (B) Micro-CT angiography results for mean vascular volume/tumor volume ± SEM 24 hours post-treatment (control, $n = 9$; B20.4.1.1, $n = 10$; GDC-0980, $n = 10$). (C) Representative MECA-32 IHC images from the same groups and (D) the corresponding group estimates for mean vascular fraction (%) = (vascular area/viable tumor area) × 100 ± SEM. *$P < .05$, **$P < .01$, ***$P < .001$ compared to control using Dunnett's method.

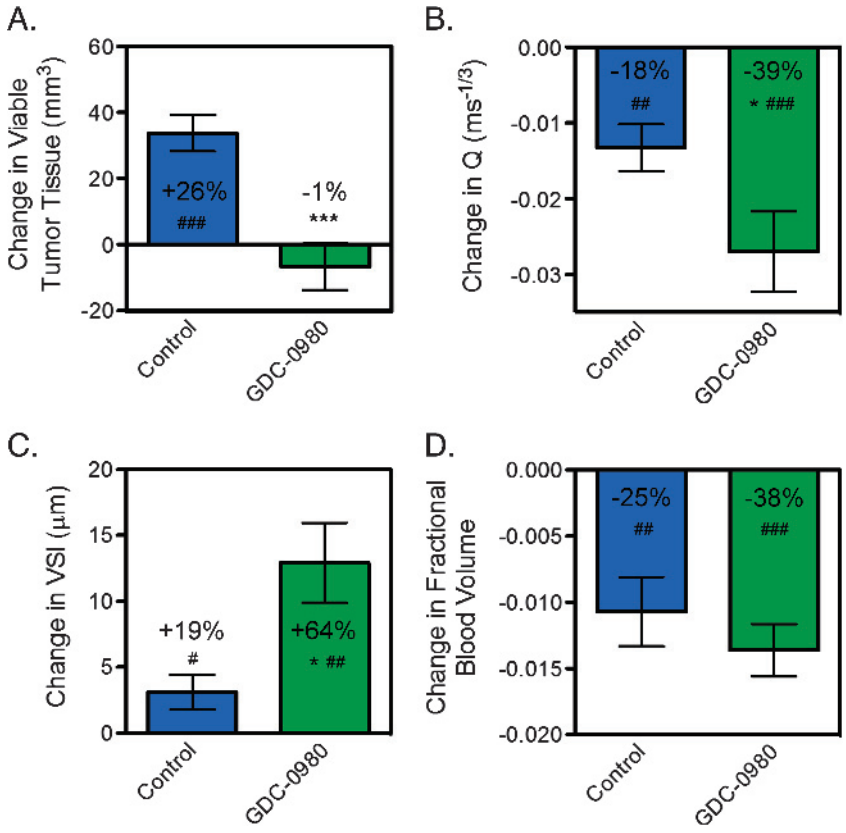

Figure 3. Inhibition of PI3K and mTORC1/C2 results in a significant loss of functional vessels in the HM-7 colorectal cancer xenograft model. (A–D) VSI MRI–derived raw change in (A) viable tumor volume, (B) *Q*, which is proportional to vessel density, (C) VSI, and (D) fractional BV 24 hours post-treatment with 10 mg/kg GDC-0980 or MCT (control); mean ± SEM, $n = 9$/group. $^{*}P < .05$, $^{***}P < .001$ compared to control using unpaired *t* test assuming unequal variances. $^{\#}P < .05$, $^{\#\#}P < .01$, $^{\#\#\#}P < .001$ *versus* pre-treatment by paired *t* test.

[25] was performed on HM-7 tumor xenografts pre-treatment and post-treatment with 10 mg/kg GDC-0980. Within 24 hours, GDC-0980 suppressed the growth of viable tumor relative to control (control: 34 ± 6 mm^3; GDC-0980: −7 ± 7 mm^3, $P < .001$; Figure 3*A*). Although, GDC-0980 did not produce a significant change in percent necrosis relative to control after 24 hours of treatment (control: −9.7 ± 1.1%; GDC-0980: −12.7 ± 1.3%, $P = .11$). Structurally, the vessel density–related parameter, *Q*, was significantly decreased following GDC-0980 treatment compared to the control (control: −0.013 ± 0.003 $ms^{-1/3}$; GDC-0980: −0.027 ± 0.005 $ms^{-1/3}$, $P < .05$; Figure 3*B*). In addition, GDC-0980 treatment resulted in an increase in mean vessel size (relative to pre-treatment estimates) that was three-fold greater than the changes observed in the control tumors (control: 3.1 ± 1.3 µm; GDC-0980: 12.9 ± 3.0 µm, $P < .05$; Figure 3*C*). However, fractional BV changes for GDC-0980 did not differ from control (Figure 3*D*), which may be attributed to a combined loss of vessels and an increase in vessel size. Collectively, the VSI MRI imaging data suggest that a loss of small functional vessels results in a decrease in vascular density and an increase in mean vessel size after GDC-0980 treatment.

GDC-0980 Strongly Alters Vascular Function

To determine functional changes within the vascular structure after GDC-0980 treatment, multispectral DCE-MRI was employed to elucidate effects on perfusion/permeability by measuring the volume transfer constant (K^{trans}), extravascular extracellular space (v_e), and fractional plasma volume (v_p) within the viable tumor [23]. GDC-0980 treatment suppressed viable tumor growth of HM-7 tumors by 24 hours (control: 24.1 ± 3.9 mm^3; GDC-0980: 10.6 ± 4.3 mm^3, $P < .05$) but not at 4 hours (control: 4.7 ± 3.2 mm^3; GDC-0980: −1.5 ± 3.5 mm^3, $P = .204$; Figure 4, *A* and *B*). GDC-0980 did not produce a significant change in percent necrosis relative to control at 4 hours (control: −5.5 ± 3.9%; GDC-0980: 0.6 ± 4.8%, $P = .34$) nor at 24 hours (control: −9.0 ± 4.1%; GDC-0980: −10.0 ± 2.1%, $P = .83$). However, 4 hours post-treatment, GDC-0980 reduced K^{trans} relative to pre-treatment estimates and relative to the changes observed in the control group (control: 2.9 ± 7.4%; GDC-0980: −28.1 ± 3.9%, $P < .01$; Figure 4, *A* and *C*). This reduction persisted for 24 hours (control: 4.1 ± 6.6%; GDC-0980: −36.0 ± 6.1%, $P < .001$) post-treatment indicating decreased delivery of the contrast agent due to effects on blood flow and/or vascular permeability. Additionally, GDC-0980 treatment increased v_e at 4 (control: −13.8 ± 4.9%; GDC-0980: 21.5 ± 6.4%, $P < .001$) and 24 hours (control: −11.8 ± 4.6%; GDC-0980: 28.2 ± 11%, $P < .01$, Figure 4*D*) relative to changes observed in the control group. However, differences between control and treated groups were not observed in v_p at either time point (Figure 4*E*).

Since the DCE-MRI parameter K^{trans} is sensitive to both blood flow and permeability, DCE-U/S imaging with an intravascular contrast agent was used to assess the effects of GDC-0980 on blood flow in HM-7 tumor–bearing mice. GDC-0980 significantly reduced blood flow within the enhancing region of the tumor relative to

pre-treatment values and to changes observed in the control group (control: −11.5 ± 7.5%; GDC-0980: −69.2 ± 4.9%, $P < .001$; Figure 5, *A* and *B*), consistent with an increase in vasoconstriction due to inhibition of VEGF activity, a known vasodilator [43]. Furthermore, GDC-0980 produced a significant decrease in the enhancement factor (E_f; control: −7.8 ± 3.1%; GDC-0980: −53.1 ± 5.7%, $P < .001$; Figure 5*C*), which is consistent with a reduction in vascular density.

Inhibition of PI3K Directly Reduces Endothelial Cell Migration, Sprout Formation, and Viability

Since treatment with GDC-0980 resulted in a robust antiangiogenic response, the question arises whether the effects on vascular structure and functions were due to inhibition of PI3K, mTOR, or both. To test this hypothesis, studies were performed with a small molecule inhibitor that selectively targets class I PI3K (GNE-490) and has similar biochemical and cellular potencies to GDC-0980

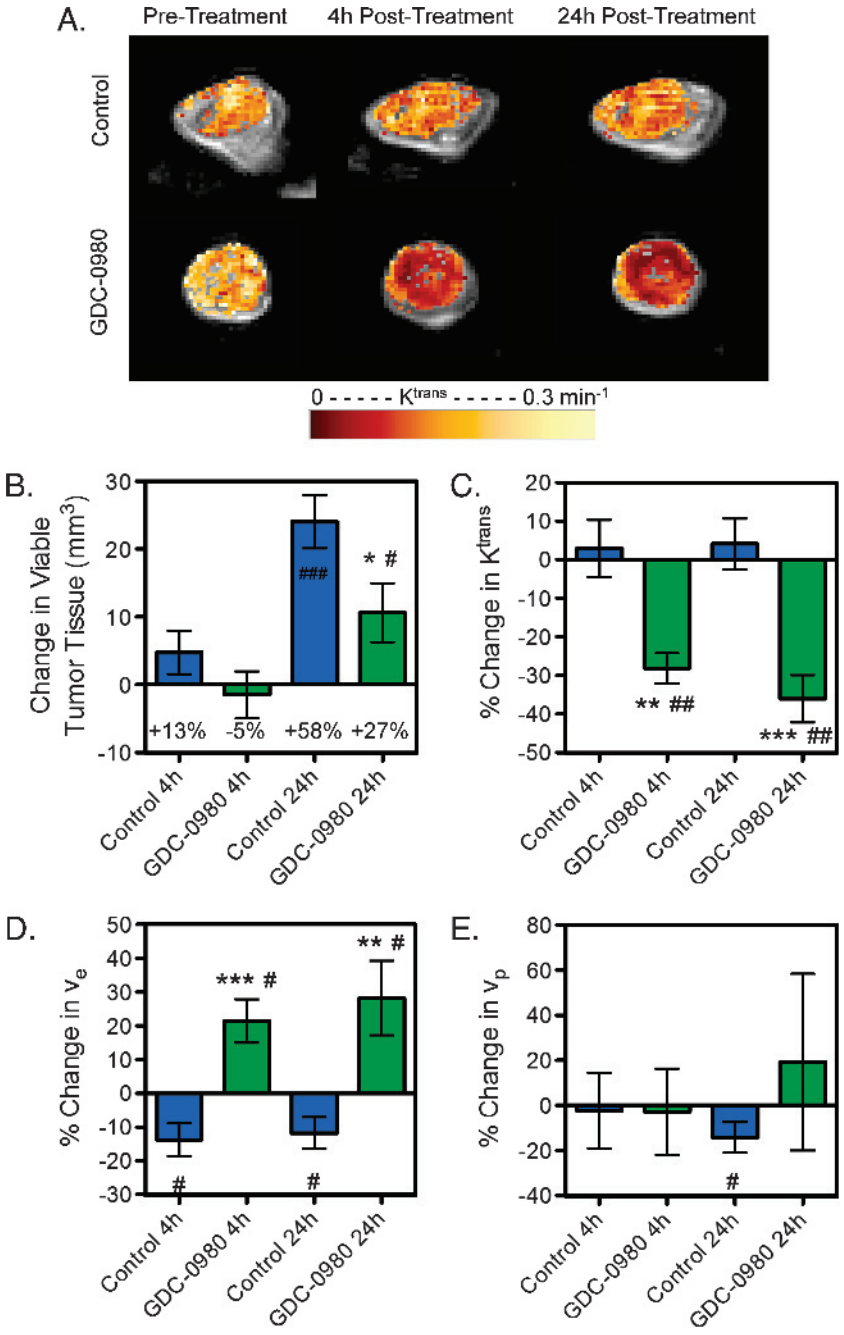

Figure 4. Inhibition of PI3K and mTORC1/C2 affects vascular function in HM-7 xenograft model as assessed by DCE-MRI. (A) Representative false-colorized DCE-MRI K^{trans} maps for the viable tumor regions pre-treatment as well as 4 and 24 hours post-treatment with MCT vehicle control ($n = 11$) or 7.5 mg/kg GDC-0980 ($n = 9$) overlaid onto the corresponding proton density image. (B–E) Multispectral DCE-MRI–derived (B) change in viable tumor volume, (C) percent change in K^{trans}, (D) percent change in v_e, and (E) percent change in v_p for tumor-bearing mice described in A (mean ± SEM). $^{*}P < .05$, $^{**}P < .01$, $^{***}P < .001$ *versus* control by unpaired *t* test assuming unequal variances; $^{\#}P < .05$, $^{\#\#}P < .01$, $^{\#\#\#}P < .001$ *versus* pre-treatment by paired *t* test.

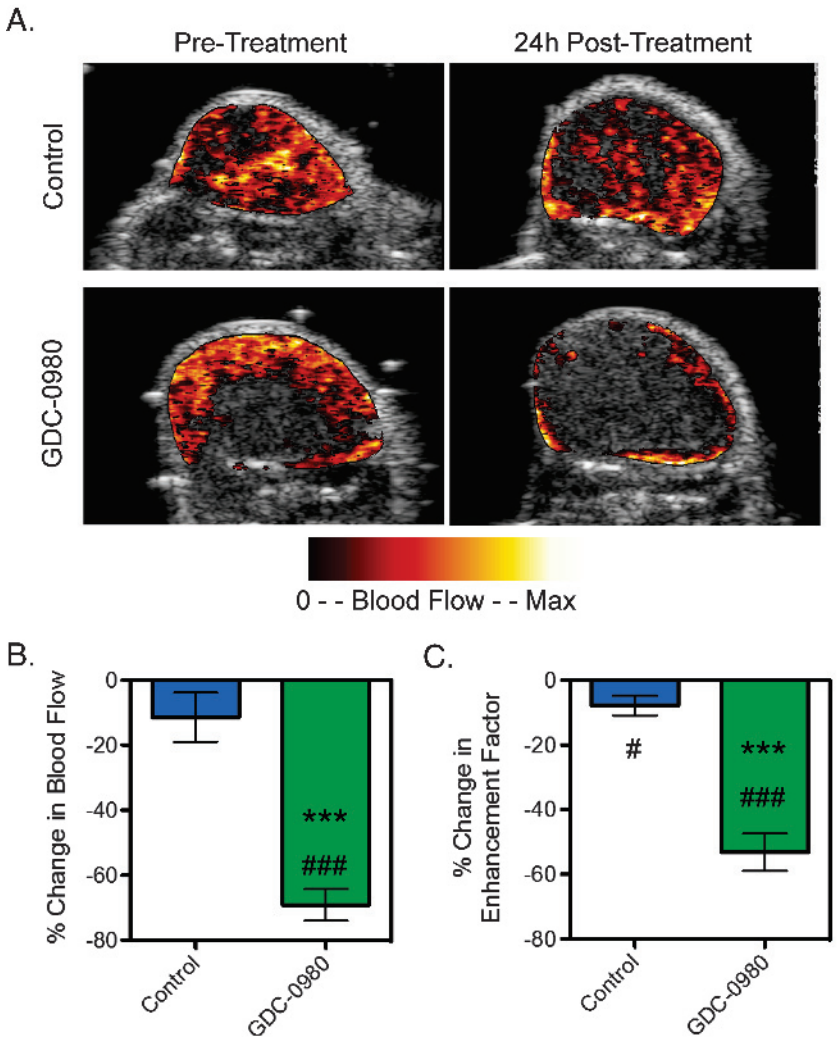

Figure 5. Inhibition of PI3K and mTORC1/C2 affects vascular function in the HM-7 xenograft model as assessed by DCE-U/S. (A) Representative false-colorized DCE-U/S blood flow maps overlaid onto their anatomic images pre-treatment or 24 hours post-treatment with MCT vehicle (control) or 7.5 mg/kg GDC-0980 (n = 6/group). (B and C) Percent change in DCE-U/S–derived (B) blood flow in the enhancing tumor regions and (C) enhancement factor for tumor-bearing mice described in A (mean ± SEM). $^{***}P < .001$ *versus* control by unpaired t test assuming unequal variances; $^{\#}P < .05$, $^{\#\#\#}P < .001$ *versus* pre-treatment by paired t test.

but does not target mTORC1/C2 [26]. In addition, GNE-490 has similar drug exposures in immunocompromised mice to GDC-0980 that is ideal for accurately comparing the pharmacodynamic responses and efficacy of both drugs *in vivo* [28,30].

Initially, the direct effects of GNE-490 and GDC-0980 on endothelial cells were compared *in vitro* using HUVECs as a model. Compared to GDC-0980, GNE-490 suppressed the phosphorylation of PI3K pathway biomarkers (pAkt, pS6RP, and p4EBP) and decreased phosphorylation of eNOS to similar degrees (Figure 6*A*). In addition, GNE-490 and GDC-0980 significantly inhibited HUVEC migration by 80% and 75%, respectively, relative to control treatment after growth factor stimulation (mean cell migration index, control: 2.42 ± 0.11; GNE-490: 0.48 ± 0.06, $P < .001$; GDC-0980: 0.6 ± 0.06, $P < .001$; Figure 6*B*). To evaluate the functional consequences of the migration defect, we measured the effects of GNE-490 and GDC-0980 on endothelial sprout formation. Both GNE-490 and GDC-0980 significantly suppressed formation of elongated sprouts by 59% and 48%, respectively (mean total vessel outgrowth, control: 2175.45 ± 48.92; GNE-490: 901.14 ± 60.95, $P < .001$; GDC-0980: 1121.97 ± 56.73, $P < .001$; bevacizumab: 894.1 ± 90.14, $P < .001$; Figure 6, *C* and *D*). Moreover, the inhibitory effects on sprouting were similar between anti-human VEGF-A (bevacizumab), GNE-490, and GDC-0980 (Figure 6, *C* and *D*). Consistent with a less motile phenotype, morphologically, the sprouts that remained after GNE-490 and GDC-0980 treatment contained blunted tips with few filopodia when compared to untreated cells (Figure 6*C*, inset). The inhibition of endothelial cell sprouting by treatment with either GNE-490 or GDC-0980 may, in part, be due to increased apoptotic cell death (mean apoptotic index, control: 1.25 ± 0.19; GNE-490: 3.91 ± 0.7, $P < .01$; GDC-0980: 3.75 ± 0.49, $P < .01$; Figure 6*E*).

Selective Inhibition of PI3K Is Sufficient for Reducing Vascular Density

Given that PI3K inhibition by GNE-490 was sufficient to directly reduce endothelial cell migration, survival, and sprouting *in vitro*, GNE-490 effects on vascular structure were evaluated *in vivo*.

Vascular density assessed by micro-CT angiography of HM-7 tumors was reduced relative to control following treatment with GNE-490, which was comparable to GDC-0980 and B20.4.1.1 (control: 4.8 ± 0.32%; GNE-490: 2.5 ± 0.2%; GDC-0980: 2.5 ± 0.28%, B20.4.1.1: 2.6 ± 0.23%; $P < .001$ *vs* control for all treatments; Figure 7, *A* and *B*). In addition, GNE-490 reduced vascular density in another anti–VEGF-A sensitive xenograft model (NCI-PC3 prostate cancer) relative to control that was comparable to reductions produced

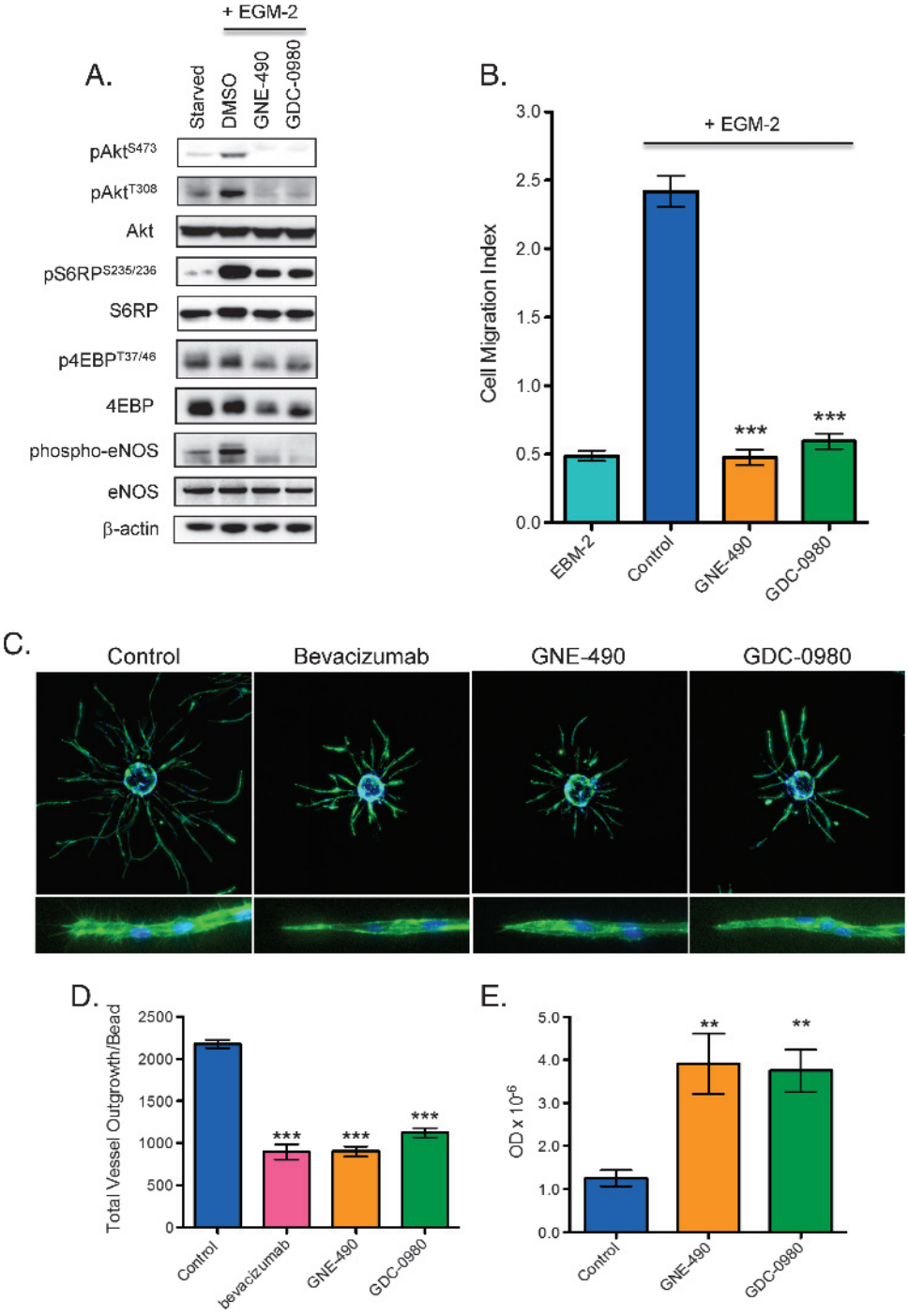

Figure 6. Inhibition of PI3K reduces endothelial cell migration, sprout formation, and viability *in vitro*. (A) HUVECs were stimulated with EGM-2 growth factor media for 1 hour in the presence of DMSO vehicle (control), 0.40 μM GNE-490, or 0.40 μM GDC-0980 before immunoblot analysis for PI3K pathway markers and eNOS as shown. (B) HUVEC migration was induced with EGM-2 growth factor media in the presence of DMSO (control), 0.4 μM GNE-490, or 0.4 μM GDC-0980 for 72 hours and quantified as mean ± SEM. (C) Representative images of established endothelial sprouts after treatment with 20 μg/ml control antibody (anti-ragweed), 20 μg/ml bevacizumab, 0.40 μM GNE-490, and 0.40 μM GDC-0980 for 4 days. Cells were imaged using Molecular Devices ImageXpress Micro automated microscope with a 4× S Fluor objective and (D) quantified for total vessel outgrowth/bead (mean ± SEM). (C, bottom row) Higher resolution representative images (10×) of endothelial sprout tips. (E) Endothelial cell apoptosis was measured by a nuclear ELISA assay after treatment with DMSO vehicle (control), 0.40 μM GNE-490, or 0.40 μM GDC-0980 for 48 hours and quantified as mean optical density ± SEM. $^{**}P < .01$, $^{***}P < .001$ compared to control using Dunnett's method.

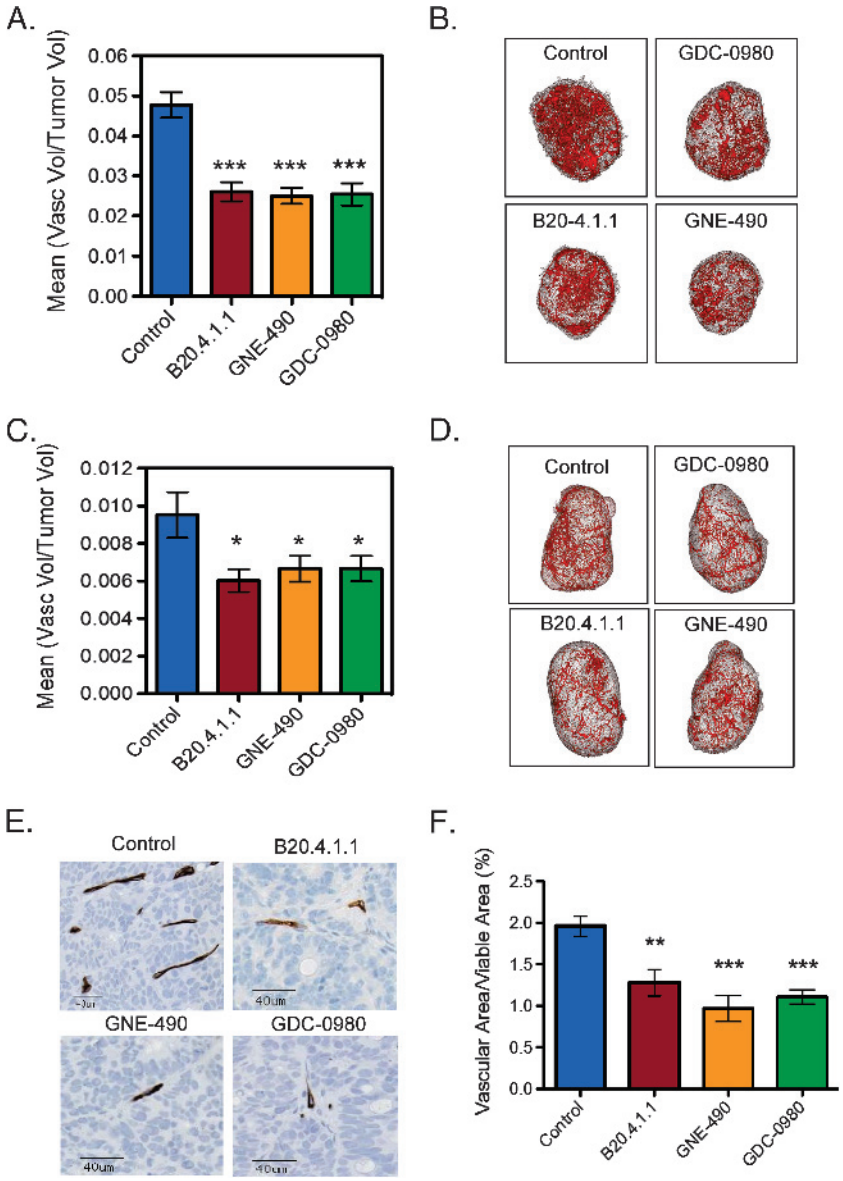

Figure 7. Inhibition of PI3K is sufficient for reducing vascular density in HM-7 and NCI-PC3 xenograft models. (A) HM-7 xenograft model: micro-CT angiography results of mean vascular volume/tumor volume ± SEM 24 hours following a single dose of MCT vehicle (control), B20.4.1.1 (10 mg/kg), GNE-490 (30 mg/kg), or GDC-0980 (10 mg/kg) (HM-7 xenograft model). (B) Representative 3D renderings of the micro-CT–derived vascular skeleton (red) overlaid onto HM-7 tumor tissue (gray) from mice described in A. (C) NCI-PC3 xenograft model: micro-CT angiography results of mean vascular volume/tumor volume ± SEM 48 hours following a single dose of MCT vehicle (control), B20.4.1.1 (10 mg/kg), GNE-490 (30 mg/kg), or GDC-0980 (10 mg/kg). (D) Representative 3D renderings of the micro-CT–derived vascular skeleton (red) overlaid onto NCI-PC3 tumor tissue (gray) from mice described in C. (E) Representative IHC images of MECA-32–positive vessels contained in HM-7 tumors after 7 days of daily treatment with MCT vehicle (control), 10 mg/kg B20.4.1.1, 30 mg/kg GNE-490, or 10 mg/kg GDC-0980 and (F) the corresponding estimates for mean vascular fraction (%) = (vascular area/viable tumor area) × 100 ± SEM, $n = 10$/group. Comparisons to control were performed using Dunnett's method; *$P < .05$, **$P < .01$, ***$P < .001$.

by GDC-0980 and B20.4.1.1 (control: 0.95 ± 0.12%; B20.4.1.1: 0.60 ± 0.06%; GDC-490: 0.67 ± 0.069%; GDC-0980: 0.67 ± 0.067%; $P < .05$ *vs* control for all treatments; Figure 7, *C* and *D*). The antivascular response was also confirmed in the HM-7 model after daily dosing of drugs for 7 days in which GDC-0980, GNE-490, and B20.4.1.1 exhibited a similar reduction in MECA-32–positive vessels (100 × VAF, control: 1.96 ± 0.12%; GDC-0980: 1.11 ± 0.09%, $P < .001$; GNE-490: 0.97 ± 0.16%, $P < .001$; B20.4.1.1: 1.28 ± 0.16%, $P < .01$; Figure 7, *E* and *F*). Moreover, the small MECA-32–positive vessels that were present 24 hours after a single dose of GDC-0980 (Figure 2*C*) were not detectable after continuous daily treatment (Figure 7*E*). The antivascular effects of GNE-490 and GDC-0980 were not due to a suppression of HM-7 tumor–derived VEGF-A secretion since GDC-0980 and GNE-490 did not significantly reduce the expression of human VEGF-A_{165} or VEGF-A_{121} isoforms relative to control levels (Figure W1).

The pharmacodynamic effects of GNE-490 was confirmed to be on-target based on a 73% reduction of pAkt (control: 0.044 ± 0.003; GNE-490: 0.012 ± 0.002, $P < .001$) and a 61% reduction in pS6RP (control: 0.69 ± 0.08; GNE-490: 0.27 ± 0.04, $P < .001$) in HM-7 tumors (Figure 8, *A* and *B*). Relative to control treatment, GNE-490

also reduced pAkt levels by 74% (control: 0.034 ± 0.002; GNE-490: 0.009 ± 0.001, $P < .001$) and reduced pS6RP levels by 69% (control: 0.55 ± 0.01; GNE-490: 0.17 ± 0.02, $P < .001$) in NCI-PC3 tumors (Figure 8, *C* and *D*). Given that pS6RP is a proximal biomarker for mTOR inhibition, a significant reduction in pS6RP levels was also observed with GDC-0980 when compared to GNE-490 in both HM-7 (GDC-0980: 0.14 ± 0.03, $P < .05$) and NCI-PC3 (GDC-0980: 0.11 ± 0.01, $P < .05$) xenograft models (Figure 8, *B* and *D*). However, the significant reduction of pAkt and pS6RP by GNE-490 in both xenograft models demonstrates that robust PI3K pathway suppression can be achieved at the level of PI3K inhibition. The latter findings correlated well with the antitumor effects of GNE-490 in which drug

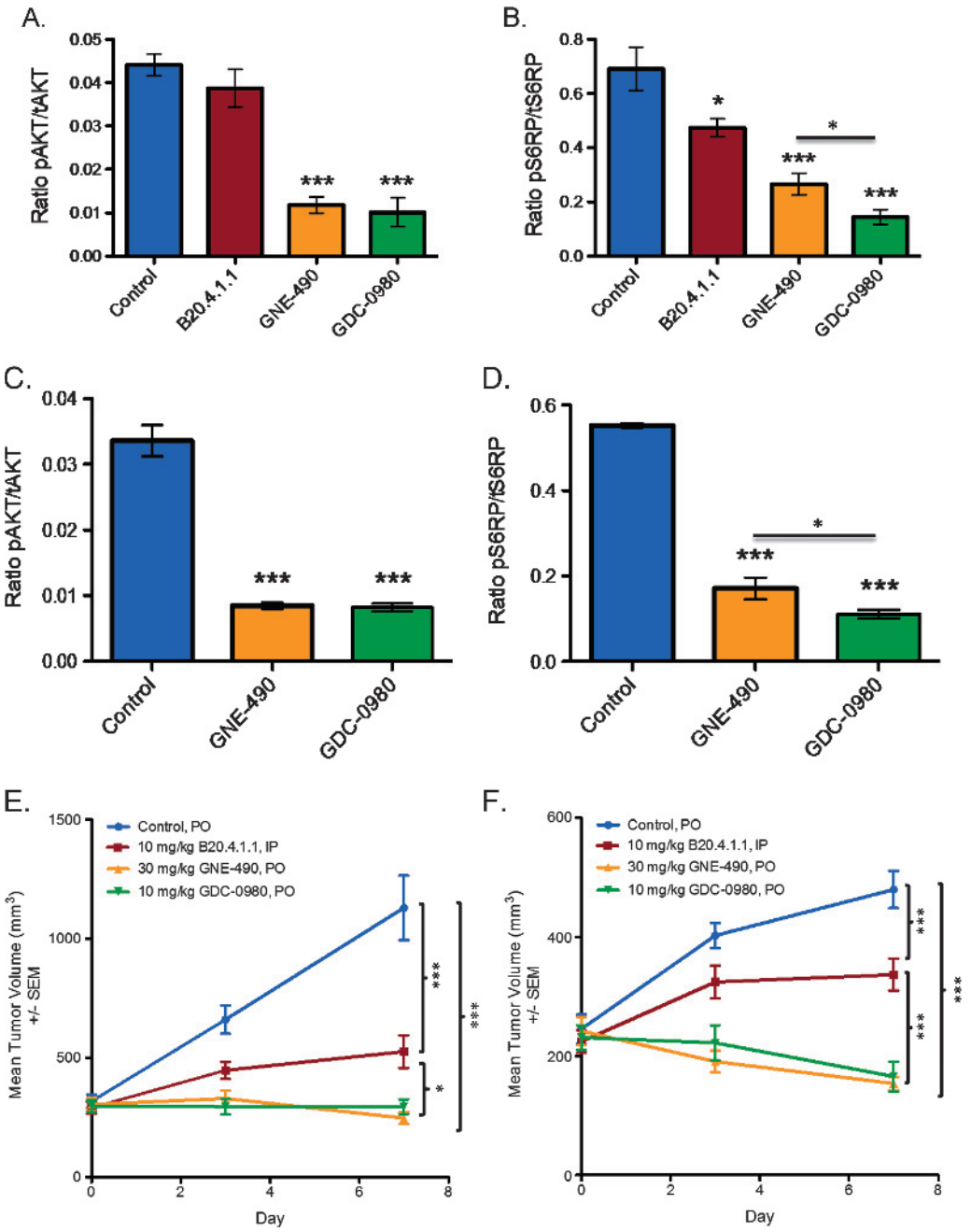

Figure 8. GNE-490 reduces pAkt, pS6RP, and tumor growth in HM-7 colorectal cancer and NCI-PC3 prostate cancer xenograft models. (A and B) HM-7 tumor–bearing mice ($n = 3$) were treated with a single oral dose of GDC-0980 (10 mg/kg) or GNE-490 (30 mg/kg) or i.p. dose of B20.4.1.1 (10 mg/kg) and harvested 1 hour post-dose to measure the levels of pAkt (S^{473}) normalized to tAkt (A) or pS6RP ($S^{235/236}$) normalized to tS6RP (B) using Meso Scale Discovery assays (mean ± SEM). (C and D) NCI-PC3 tumor–bearing mice ($n = 4$) were treated with a single dose of MCT vehicle (control), GDC-0980 (10 mg/kg), or GNE-490 (30 mg/kg), and tumors were harvested 1 hour post-dose to measure the levels of pAkt (S^{473}) normalized to tAkt (C) or pS6RP ($S^{235/236}$) normalized to tS6RP (D). (E and F) Mean tumor volumes from HM-7 (E) and NCI-PC3 (F) tumor–bearing mice treated daily and p.o. with MCT vehicle (control), GDC-0980 (10 mg/kg), or GNE-490 (30 mg/kg) for 7 days. B20.4.1.1 (10 mg/kg) was administered i.p. on days 1 and 7. Comparisons to control were performed using Dunnett's method; comparisons between treatment groups were performed using unpaired *t* test assuming unequal variances: *$P < .05$, **$P < .01$, ***$P < .001$.

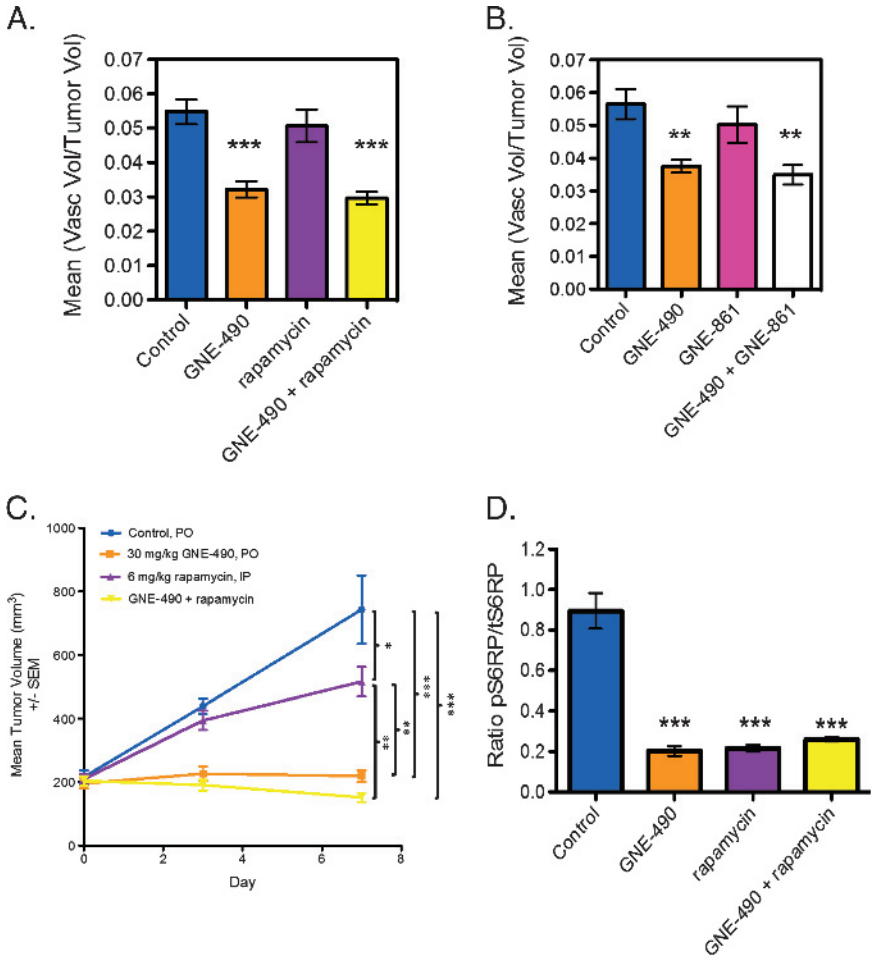

Figure 9. Combination of mTOR inhibitors with GNE-490 does not further reduce vascular density compared to GNE-490 alone in HM-7 xenograft model. (A and B) Micro-CT angiography results of mean vascular volume/tumor volume ± SEM 24 hours following a single dose of MCT vehicle (control), 30 mg/kg GNE-490, 6 mg/kg rapamycin (A), 30 mg/kg GNE-490 + 6 mg/kg rapamycin (A), 100 mg/kg GNE-861 (B), or 30 mg/kg GNE-490 + 100 mg/kg GNE-861 (B) (n = 8–10/group). (C) Mean tumor volumes for HM-7 tumor–bearing mice (n = 8) treated daily and p.o. with MCT vehicle (control), GNE-490, rapamycin, or the combination of GNE-490 and rapamycin for 7 days at the doses indicated. (D) The ratio of pS6RP ($S^{235/236}$) to tS6RP in tumors from HM-7 tumor–bearing mice (n = 4) was treated with a single oral dose of GNE-490 (30 mg/kg), rapamycin (6 mg/kg), or the combination of GNE-490 and rapamycin (mean ± SEM). Comparisons to control were performed using Dunnett's method; comparisons between treatment groups were performed using unpaired t test assuming unequal variances: *P < .05, **P < .01, ***P < .001.

treatment inhibited tumor growth by 78% in the HM-7 model (control: 1129.86 ± 135.57 mm^3; GNE-490: 246.71 ± 25.26 mm^3, P < .001; GDC-0980: 294.85 ± 30.84 mm^3, P < .001; B20.4.1.1: 525.82 ± 68.50 mm^3, P < .001) and 68% in the NCI-PC3 model (control: 479.74 ± 31.15 mm^3; GNE-490: 153.73 ± 11.22 mm^3, P < .001; GDC-0980: 165.37 ± 25.01 mm^3, P < .001; B20.4.1.1: 336.62 ± 27.08 mm^3, P < .001; Figure 8, *E* and *F*). GDC-980 inhibited HM-7 tumor growth by 74% and NCI-PC3 tumor growth by 66% and, therefore, was as efficacious as GNE-490 in both xenograft models (Figure 8, *E* and *F*). Moreover, GNE-490 was more efficacious than B20.4.1.1 in both the HM-7 (P < .05) and NCI-PC3 (P < .001) xenograft models, suggesting that selective inhibition of PI3K is sufficient to induce a combined antitumorigenic and antivascular response that translates into greater TGI when compared to drugs that target the tumor vasculature alone such as anti–VEGF-A (Figure 8, *E* and *F*).

To confirm that inhibition of PI3K was sufficient to reduce vascular density, selective mTOR inhibitors, rapamycin (mTORC1) or GNE-861 (mTORC1/C2), were combined with GNE-490 and the effects on vascular structure were evaluated in HM-7 xenografts by micro-CT angiography. Both rapamycin (control: 5.5 ± 0.36%; GNE-490: 3.2 ± 0.24%, P < .001; rapamycin: 5.1 ± 0.48%, P = .7; GDC-490 + rapamycin: 3.0 ± 0.19%, P < .001; Figure 9*A*) and GNE-861 (control: 5.7 ± 0.5%; GNE-490: 3.8 ± 0.2%, P < .01; GNE-861: 5.0 ± 0.6%, P = .55; GNE-490 + GNE-861: 3.5 ± 0.3%, P < .01; Figure 9*B*) were included in separate four-arm combination studies with GNE-490. Neither rapamycin nor GNE-861 treatment alone reduced vascular density relative to control. Moreover, the addition of rapamycin or GNE-861 to GNE-490 treatment did not reduce vascular density when compared to GNE-490 alone. Additionally, when compared with GNE-490 treatment alone, rapamycin did not significantly enhance the efficacy of GNE-490 when both drugs were combined in the HM-7 xenograft model (GNE-490: 218.97 ± 18.59 mm^3; GNE-490 + rapamycin: 161.83 ± 16.75 mm^3, P = .45; Figure 9*C*). We confirmed that, GNE-490, rapamycin and

the combination of GNE-490 and rapamycin were indeed pharmacologically active as significant reductions in pS6RP tumor levels of 76%, 75%, and 71%, respectively, were observed when compared to control levels (control: 0.89 ± 0.09; GNE-490: 0.21 ± 0.02, $P < .001$; rapamycin: 0.22 ± 0.02, $P < .001$; GNE-490 + rapamycin: 0.26 ± 0.01, $P < .001$; Figure 9*D*). Collectively, our evaluation of GNE-490 and mTOR-specific inhibitors suggests that selective inhibition of PI3K is sufficient to produce a robust antivascular response *in vivo*.

Selective Inhibition of PI3K Is Sufficient for Reducing Vascular Function

Selective inhibition of PI3K by GNE-490 on vascular function was assessed by DCE-MRI and DCE-U/S in the HM-7 xenograft tumor model. Twenty-four hours following treatment with GNE-490 or GDC-0980, viable tumor growth was reduced (control: 43.6 ± 4.9 mm^3; GNE-490: 7.2 ± 2.9 mm^3; GDC-0980: −5.3 ± 2.2 mm^3; $P < 0.001$ for both treatment groups; Figure 10, *A* and *B*). Both GNE-490 (4.0 ± 2.5%, $P < 0.01$) and GDC-0980 (1.5 ± 2.9%, $P < .05$) groups exhibited an increase in percent necrosis relative to control (−8.6 ± 2.1%) but not relative to pre-treatment values. K^{trans} was reduced within the viable tumor by GNE-490 and GDC-0980 relative to pre-treatment values and the changes observed under control treatment (control: −1.4 ± 4.9%; GNE-490: −21.5 ± 7.0%, $P < .05$; GDC-0980: −28.7 ± 5.4%, $P < .01$; Figure 10, *A* and *C*). GDC-0980 induced a reduction in v_p when compared to changes observed in the control-treated animals, whereas GNE-490 did not produce a significant response relative to control (control: −5.9 ± 8.6%; GNE-490: −21.1 ± 9.4%, $P = .321$; GDC-0980: −38.7 ± 5.7%, $P < .01$; Figure 10*D*). Relative to control, GDC-0980 produced a significant increase in v_e, while GNE-490 did not (control: −0.59 ± 5.2%; GNE-490: 14.9 ± 9.9%, $P = .2$; GDC-0980: 25.0 ± 5.0%; $P < .05$; Figure 10*E*). Although GNE-490 did not alter v_p or v_e relative to control, there were no significant differences between the GDC-0980 and GNE-490 treatment groups for any of the DCE-MRI parameters that were measured.

DCE-U/S detected a trend toward decreased blood flow in the enhancing tumor regions following treatment with GNE-490 or GDC-0980 that did not differ significantly from control (control: −1.4 ± 10.1%; GNE-490: −23.7 ± 6.0%, $P = .123$; GDC-0980: −20.7 ± 7.3%, $P = .18$; Figure 11, *A* and *B*). However, the percent change in E_f was significantly reduced by both GNE-490 and GDC-0980 relative to changes measured in the control group (control: 2.4 ± 2.3%; GNE-490: −13.8 ± 2.8, $P < .05$; GDC-0980: −16.0 ± 6.3, $P < .05$; Figure 11, *A* and *C*). There were no significant differences between GNE-490 and GDC-0980 groups for percent change in blood flow or E_f (Figure 11, *B* and *C*).

The effects of GNE-490 *versus* GDC-0980 on vascular endothelial cell function were further evaluated by FMD and NTG responses in non–tumor-bearing mice. FMD assesses the ability of endothelial cells to respond to a hypoxic challenge that leads to increased eNOS production of NO that induces vasodilation. In the NTG experiment, NTG directly stimulates vascular smooth muscle cells to induce vasodilation and bypasses any effects on endothelial cell signaling. For FMD experiments, ultrasound imaging was used to monitor FA diameter prior and after a transient occlusion of blood flow to the right leg by a rubber band cuff. Eight minutes after the FMD experiment was

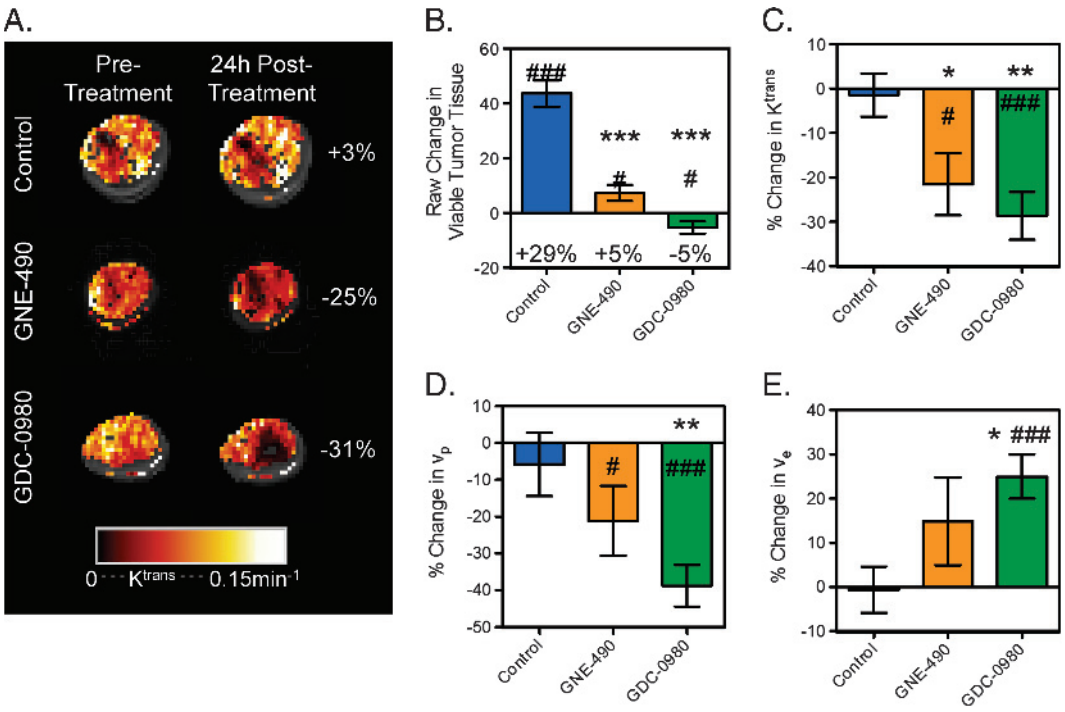

Figure 10. Inhibition of PI3K affects vascular function in HM-7 xenograft model as assessed by DCE-MRI. (A) Representative false-colorized DCE-MRI K^{trans} maps for the viable tumor regions pre-treatment as well as 24 hours post-treatment with MCT vehicle (control, $n = 14$), GNE-490 (30 mg/kg, $n = 11$), or GDC-0980 (10 mg/kg, $n = 13$) overlaid onto the corresponding proton density image (HM-7 xenograft model). The percent change from baseline is noted. (B–E) Multispectral DCE-MRI–derived (B) change in viable tumor volume, (C) percent change in K^{trans}, (D) percent change in v_p, and (E) percent change in v_e for the mice described in A (mean ± SEM). $^*P < .05$, $^{**}P < .01$, $^{***}P < .001$ compared to control using Dunnett's method; $^{\#}P < .05$, $^{\#\#}P < .01$, $^{\#\#\#}P < .001$ *versus* pre-treatment by paired *t* test.

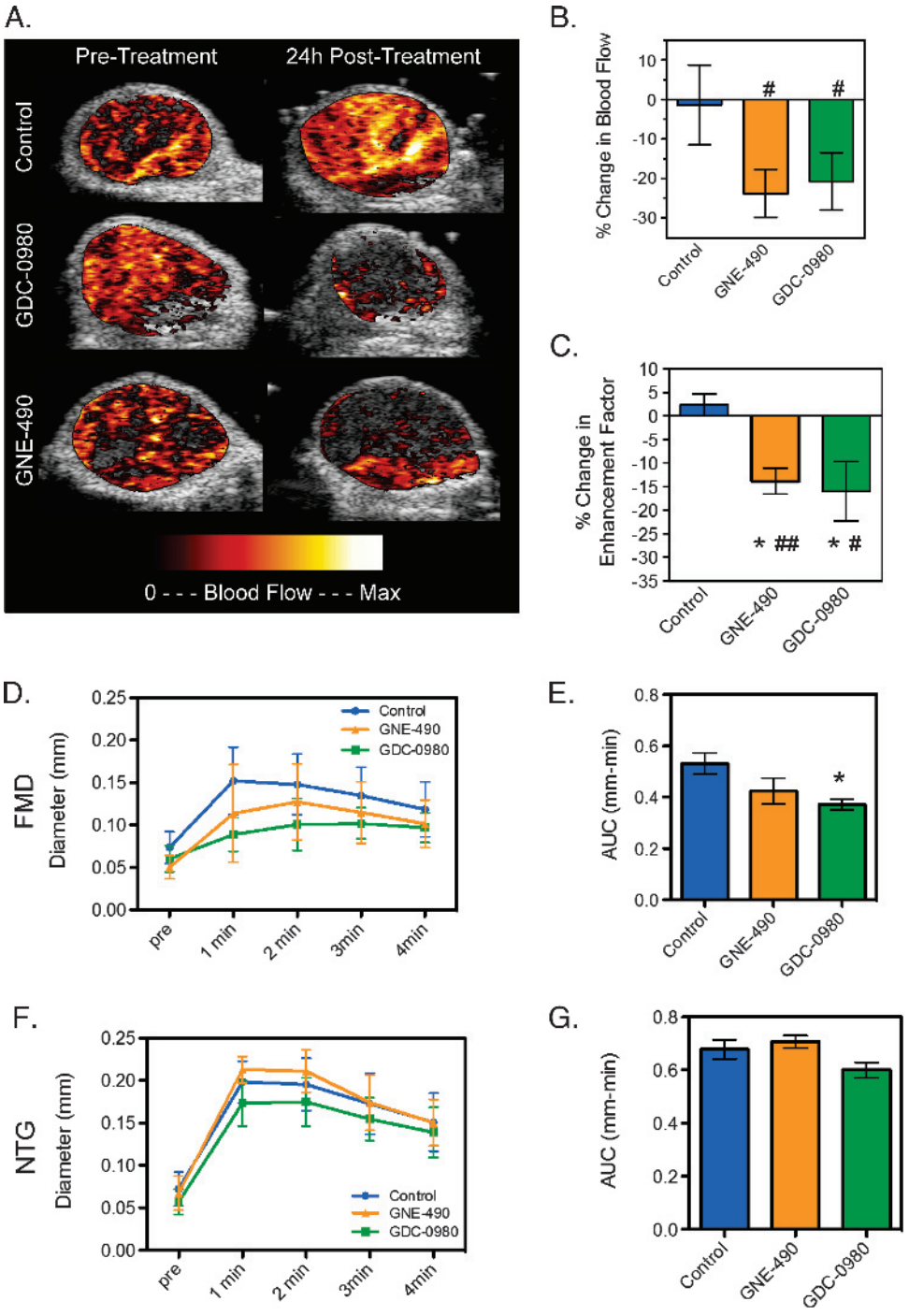

Figure 11. GNE-490 is sufficient for reducing tumor perfusion assessed by DCE-U/S, whereas GDC-0980 suppresses hypoxia-induced FMD in normal vasculature. DCE-U/S: A–C. (A) Representative false-colorized DCE-U/S blood flow maps overlaid onto their anatomic images pre-treatment or 24 hours post-treatment with MCT vehicle (control, $n = 8$), GNE-490 (30 mg/kg, $n = 7$), or GDC-0980 (10 mg/kg, $n = 8$). (B and C) Mean percent change ± SEM in DCE-U/S–derived (B) blood flow in the enhancing tumor regions and (C) enhancement factor for the mice described in A. FMD and NTG experiments: D–G. (D) Mean diameter of the FA before and following a transient (4-minute) occlusion of blood flow to the right leg 4 hours post-treatment with 30 mg/kg GNE-490, 10 mg/kg GDC-0980, or MCT (control) ± SEM ($n = 9$/group). (E) Area under the curve for the plots in D (mean ± SEM). (F) Mean diameter of the FA of the left leg before and following NTG-mediated dilation 4 hours post-treatment with 30 mg/kg GNE-490, 10 mg/kg GDC-0980, or MCT (control) ± SEM ($n = 9$/group). (G) Area under the curve for the plots in E (mean ± SEM). *$P < .05$ compared to control using Dunnett's method; $^{\#}P < .05$, $^{\#\#}P < .01$ *versus* pre-treatment by paired *t* test.

completed, an NTG-mediated dilation/endothelial cell–independent experiment was performed on the opposite leg. GDC-0980 strongly suppressed the FMD response, whereas GNE-490 exhibited a modest trend (Figure 11, *D* and *E*). The differences between GNE-490 and GDC-0980 FMD responses were insignificant and neither drug was able to suppress the ability of NTG to directly stimulate vascular smooth muscle cells to promote vasodilation (Figure 11, *F* and *G*). The FMD study demonstrates that GDC-0980 and, possibly, GNE-490, to a

lesser extent, were able to specifically suppress eNOS production of NO in endothelial cells.

Discussion

In this study, selective class I PI3K, dual PI3K/mTOR, and mTOR small molecule inhibitors were evaluated using multimodal imaging techniques to elucidate the overall contributions of PI3K *versus* PI3K and mTOR activity on tumor vascular structure and function in colorectal and prostate cancer xenograft models that are sensitive to anti–VEGF-A treatment. Initially, these studies focused on the dual PI3K/mTOR inhibitor, GDC-0980, to determine its effects on vascular structure and function when both PI3K and mTOR are simultaneously blocked in the HM-7 colorectal cancer xenograft model. On the basis of *ex vivo* micro-CT angiography, a single dose of GDC-0980 produced a strong antivascular response comparable to anti–VEGF-A monotherapy. In addition, this robust antivascular effect was confirmed by treatment of HM-7 xenografts with daily (7 days) doses of GDC-0980 and resulted in a decrease in MECA-32–positive endothelial cells that was comparable to anti–VEGF-A monotherapy. GDC-0980 treatment also induced a robust suppression of PI3K proximal and distal pathway markers, such as pAkt and pS6RP, respectively, in tumors. This tumor cell response did not result in acute tumor cell killing since multispectral MRI did not detect a robust increase in percent necrosis after 24 hours of treatment. However, compared to anti–VEGF-A, GDC-0980 treatment resulted in greater TGI likely due to both PI3K pathway inhibition in tumor cells and a strong antivascular effect on the endothelium. The compromised vascular structure induced by GDC-0980 corresponded to diminished function *in vivo* since a strong decrease in the DCE-MRI parameter, K^{trans}, was observed after a single dose, indicating a rapid alteration of vascular permeability and/or blood flow in the viable tumor region. In addition, DCE-U/S and VSI MRI confirmed a reduction in functional perfusion and vessel density, respectively, after GDC-0980 treatment. Thus, these initial studies led to the conclusion that inhibition of both PI3K and mTOR by GDC-0980 results in potent antivascular and antitumorigenic effects that translate into greater efficacy when compared to anti–VEGF-A treatment. The effects on vascular function by GDC-0980 corroborates the work of Schnell et al. where treatment of the BN472 mammary carcinoma allograft model with BEZ-235, a dual PI3K/mTOR inhibitor, inhibited microvessel permeability, reduced tumor interstitial pressure, and decreased K^{trans} [19]. However, the study of Schnell et al. did not evaluate the effects of the dual PI3K/mTOR inhibition on vessel structure, whereas our evaluation of GDC-0980 by micro-CT angiography and VSI MRI identified a strong structural antivascular response that is produced by this class of drugs.

Initially, evaluating the antivascular effects of GDC-0980 established a benchmark that permitted further interrogation of PI3K alone using selective inhibitors such as GNE-490 that has comparable potency against PI3K and drug exposures in mice to GDC-0980 [28]. The potent antivascular effects of GNE-490 were confirmed in the HM-7 and NCI-PC3 xenograft models by micro-CT angiography and resulted in a significant reduction in vascular density that was similar to GDC-0980. The impact of GNE-490 on an array of functional vascular end points did not differ significantly from responses observed with GDC-0980, suggesting that PI3K inhibition was sufficient to inhibit tumor vascular function. Moreover, the combination of GNE-490 with mTOR inhibitors, rapamycin or GNE-861, did not further reduce vascular density nor enhance the efficacy of GNE-490. The comparable antivascular activity of GNE-490 and GDC-0980 *in vivo* is likely due to a direct effect on vascular endothelial cells since both drugs suppressed PI3K pathway markers leading to reduced endothelial cell migration and sprouting and increased cell death *in vitro*. Collectively, these data demonstrate that selective PI3K inhibition is sufficient to induce potent antivascular responses that combine with strong antitumorigenic activity to maximize efficacy *in vivo*.

There are some differences in the functional imaging results that may be due to technical limitations. Although there were no significant differences between DCE-MRI, DCE-U/S, and FMD responses for GNE-490 and GDC-0980 treatment, GDC-0980 produced significant responses in five end points (K^{trans}, v_p, v_e, E_f, and FMD AUC), whereas GNE-490 generated significant responses in two end points (K^{trans} and E_f). This may be due to limitations in precisely matching exposures throughout the treatment window, where functional end points may be very sensitive to drug levels at the time of the imaging exam. Another question arises from the differences between the two DCE-MRI studies, namely, lack of a GDC-0980 v_p response in the first study and a strong GDC-0980 v_p response in the second. This may be due to the use of an optimized DCE-MRI protocol in the second study that provided an improved temporal resolution yielding a more accurate estimate of v_p.

Inactivation of the p110α isoform of class I PI3K by genetic knockdown or expression of a kinase dead mutant (D933A) in immunocompetent mice supports the strong antivascular effects observed when PI3K is inhibited [18]. Compared to p110β and δ, p110α activity is essential for vascular development as evidenced by severe defects in angiogenic sprouting and remodeling, leading to embryonic lethality at E12.5 [18]. Moreover, treatment of immortalized cardiac endothelial cells *in vitro* with a p110α selective inhibitor, PI-103, resulted in VEGF-A–dependent decreased tube formation [18]. Thus, p110α may be sufficient to regulate VEGF-A developmental angiogenesis and, in part, supports our antivascular observations in tumors treated with GNE-490.

Modulation of the tumor vasculature by the selective class I PI3K inhibitor, GDC-0941, has recently been shown to result in increased delivery of chemotherapeutic drugs through a vasculature normalization mechanism [44]. In these studies, oral administration of GDC-0941 in SQ20B human head and neck tumor xenografts resulted in increased perfusion, as measured by 3D power Doppler ultrasound [44]. Structurally, treatment with GDC-0941 produced vascular remodeling or normalization characterized by vessels that were less tortuous and longer in length compared to control animals [44]. This induction of vascular normalization led to increased delivery of doxorubicin and increased efficacy when combined with GDC-0941. While the results of Qayum et al. [44] differ from our findings with regard to reduced vascular function by GNE-490, it should be noted that doses of GDC-0941 were nonefficacious in the SQ20B xenograft model. Therefore, differential vascular responses (normalization *vs* antivascular) may be observed with PI3K inhibitors depending on the doses (nonefficacious *vs* efficacious) administered in these preclinical xenograft models.

Advancement of selective PI3K inhibitors in clinical development can be guided by the ability to rapidly assess their pharmacodynamic activity directly in tumors. *In vivo* imaging techniques offer an attractive alternative to serial biopsies because they are noninvasive and provide whole-tumor coverage making them less prone to sampling errors. While FDG-PET has proven successful at detecting rapid alterations

in tumor glucose metabolism following therapy [45], the observed hyperglycemia that has been noted with PI3K inhibitors confounds interpretation of the imaging data [39]. Thus, an alternative approach to assess the pharmacodynamic activity of PI3K or dual PI3K/mTOR inhibitors, independent of tumor genotypes, involves imaging drug effects on tumor vasculature. This study focused on an array of preclinical imaging techniques that were successfully employed to evaluate the effects of PI3K and dual PI3K/mTOR inhibitors on tumor vascular structure and function, the majority of which can be used in clinical development (VSI MRI, DCE-MRI, and DCE-U/S) [35,46,47]. DCE-MRI has been widely employed as a pharmacodynamic end point for antiangiogenic agents and a number of clinical DCE-MRI studies have been performed to evaluate antiangiogenic and antivascular agents [35]. In this study, PI3K and dual PI3K/mTOR inhibitors demonstrated a robust DCE-MRI response characterized by a strong decrease in K^{trans} attributed to changes in blood flow and/or permeability. It is also noteworthy that these inhibitors generated antivascular imaging responses that were comparable to antiangiogenic drugs, such as antibodies to VEGF-A [22,25]. On the basis of DCE-MRI's clinical success in monitoring antiangiogenic agents and the data presented here, DCE-MRI has strong potential to provide a robust and quantitative means to monitor the pharmacodynamic activity of PI3K inhibitors for testing in cancer patients and, accordingly, has been included as an end point in the clinical development of GDC-0980 [48].

In conclusion, PI3K inhibition is sufficient to generate physiological and structural changes, characteristic of a robust antivascular response. In addition, quantitative microvascular imaging techniques can be employed to effectively monitor the antivascular responses induced by PI3K and dual PI3K/mTOR inhibitors *in vivo*, thereby providing powerful tools to assess the pharmacodynamic activity of these drugs in patients.

Acknowledgments

The authors thank the *in vivo* cell culture and dosing groups at Genentech for their support.

References

[1] Hanahan D and Weinberg RA (2000). The hallmarks of cancer. *Cell* **100**, 57–70.

[2] Ferrara N and Henzel WJ (1989). Pituitary follicular cells secrete a novel heparin-binding growth factor specific for vascular endothelial cells. *Biochem Biophys Res Commun* **161**, 851–858.

[3] Leung DW, Cachianes G, Kuang WJ, Goeddel DV, and Ferrara N (1989). Vascular endothelial growth factor is a secreted angiogenic mitogen. *Science* **246**, 1306–1309.

[4] Keck PJ, Hauser SD, Krivi G, Sanzo K, Warren T, Feder J, and Connolly DT (1989). Vascular permeability factor, an endothelial cell mitogen related to PDGF. *Science* **246**, 1309–1312.

[5] Bates DO and Curry FE (1996). Vascular endothelial growth factor increases hydraulic conductivity of isolated perfused microvessels. *Am J Physiol* **271**, H2520–H2528.

[6] Hurwitz H, Fehrenbacher L, Novotny W, Cartwright T, Hainsworth J, Heim W, Berlin J, Baron A, Griffing S, Holmgren E, et al. (2004). Bevacizumab plus irinotecan, fluorouracil, and leucovorin for metastatic colorectal cancer. *N Engl J Med* **350**, 2335–2342.

[7] Cabebe E and Wakelee H (2006). Sunitinib: a newly approved small-molecule inhibitor of angiogenesis. *Drugs Today (Barc)* **42**, 387–398.

[8] Escudier B, Eisen T, Stadler WM, Szczylik C, Oudard S, Siebels M, Negrier S, Chevreau C, Solska E, Desai AA, et al. (2007). Sorafenib in advanced clear-cell renal-cell carcinoma. *N Engl J Med* **356**, 125–134.

[9] Ferrara N, Gerber HP, and LeCouter J (2003). The biology of VEGF and its receptors. *Nat Med* **9**, 669–676.

[10] Olsson AK, Dimberg A, Kreuger J, and Claesson-Welsh L (2006). VEGF receptor signalling—in control of vascular function. *Nat Rev Mol Cell Biol* **7**, 359–371.

[11] Cantley LC (2002). The phosphoinositide 3-kinase pathway. *Science* **296**, 1655–1657.

[12] Karakas B, Bachman KE, and Park BH (2006). Mutation of the PIK3CA oncogene in human cancers. *Br J Cancer* **94**, 455–459.

[13] Samuels Y, Wang Z, Bardelli A, Silliman N, Ptak J, Szabo S, Yan H, Gazdar A, Powell SM, Riggins GJ, et al. (2004). High frequency of mutations of the *PIK3CA* gene in human cancers. *Science* **304**, 554.

[14] Oikawa T and Shimamura M (1996). Potent inhibition of angiogenesis by wortmannin, a fungal metabolite. *Eur J Pharmacol* **318**, 93–96.

[15] Hu L, Hofmann J, and Jaffe RB (2005). Phosphatidylinositol 3-kinase mediates angiogenesis and vascular permeability associated with ovarian carcinoma. *Clin Cancer Res* **11**, 8208–8212.

[16] Zhao YW, Jin L, Li ZM, Zhao CJ, Wei YQ, and Yang HS (2011). Enhanced antitumor efficacy by blocking activation of the phosphatidylinositol 3-kinase/Akt pathway during anti-angiogenesis therapy. *Cancer Sci* **102**, 1469–1475.

[17] Fang J, Ding M, Yang L, Liu LZ, and Jiang BH (2007). PI3K/PTEN/AKT signaling regulates prostate tumor angiogenesis. *Cell Signal* **19**, 2487–2497.

[18] Graupera M, Guillermet-Guibert J, Foukas LC, Phng LK, Cain RJ, Salpekar A, Pearce W, Meek S, Millan J, Cutillas PR, et al. (2008). Angiogenesis selectively requires the p110α isoform of PI3K to control endothelial cell migration. *Nature* **453**, 662–666.

[19] Schnell CR, Stauffer F, Allegrini PR, O'Reilly T, McSheehy PM, Dartois C, Stumm M, Cozens R, Littlewood-Evans A, Garcia-Echeverria C, et al. (2008). Effects of the dual phosphatidylinositol 3-kinase/mammalian target of rapamycin inhibitor NVP-BEZ235 on the tumor vasculature: implications for clinical imaging. *Cancer Res* **68**, 6598–6607.

[20] Mendel DB, Laird AD, Xin X, Louie SG, Christensen JG, Li G, Schreck RE, Abrams TJ, Ngai TJ, Lee LB, et al. (2003). *In vivo* antitumor activity of SU11248, a novel tyrosine kinase inhibitor targeting vascular endothelial growth factor and platelet-derived growth factor receptors: determination of a pharmacokinetic/pharmacodynamic relationship. *Clin Cancer Res* **9**, 327–337.

[21] Wedge SR, Kendrew J, Hennequin LF, Valentine PJ, Barry ST, Brave SR, Smith NR, James NH, Dukes M, Curwen JO, et al. (2005). AZD2171: a highly potent, orally bioavailable, vascular endothelial growth factor receptor-2 tyrosine kinase inhibitor for the treatment of cancer. *Cancer Res* **65**, 4389–4400.

[22] O'Connor JP, Carano RA, Clamp AR, Ross J, Ho CC, Jackson A, Parker GJ, Rose CJ, Peale FV, Friesenhahn M, et al. (2009). Quantifying antivascular effects of monoclonal antibodies to vascular endothelial growth factor: insights from imaging. *Clin Cancer Res* **15**, 6674–6682.

[23] Berry LR, Barck KH, Go MA, Ross J, Wu X, Williams SP, Gogineni A, Cole MJ, Van Bruggen N, Fuh G, et al. (2008). Quantification of viable tumor microvascular characteristics by multispectral analysis. *Magn Reson Med* **60**, 64–72.

[24] Shojaei F, Wu X, Zhong C, Yu L, Liang XH, Yao J, Blanchard D, Bais C, Peale FV, van Bruggen N, et al. (2007). Bv8 regulates myeloid-cell-dependent tumour angiogenesis. *Nature* **450**, 825–831.

[25] Ungersma SE, Pacheco G, Ho C, Yee SF, Ross J, van Bruggen N, Peale FV Jr, Ross S, and Carano RA (2010). Vessel imaging with viable tumor analysis for quantification of tumor angiogenesis. *Magn Reson Med* **63**, 1637–1647.

[26] Sutherlin DP, Sampath D, Berry M, Castanedo G, Chang Z, Chuckowree I, Dotson J, Folkes A, Friedman L, Goldsmith R, et al. (2010). Discovery of (thienopyrimidin-2-yl)aminopyrimidines as potent, selective, and orally available pan-PI3-kinase and dual pan-PI3-kinase/mTOR inhibitors for the treatment of cancer. *J Med Chem* **53**, 1086–1097.

[27] Koehler MF, Bergeron P, Blackwood E, Bowman KK, Chen YH, Deshmukh G, Ding X, Epler J, Lau K, Lee L, et al. (2012). Potent, selective, and orally bioavailable inhibitors of the mammalian target of rapamycin kinase domain exhibiting single agent antiproliferative activity. *J Med Chem* **55**, 10958–10971.

[28] Sutherlin DP, Bao L, Berry M, Castanedo G, Chuckowree I, Dotson J, Folks A, Friedman L, Goldsmith R, Gunzner J, et al. (2011). Discovery of a potent, selective, and orally available class I phosphatidylinositol 3-kinase (PI3K)/mammalian target of rapamycin (mTOR) kinase inhibitor (GDC-0980) for the treatment of cancer. *J Med Chem* **54**, 7579–7587.

[29] Wallin JJ, Edgar KA, Guan J, Berry M, Prior WW, Lee L, Lesnick JD, Lewis C, Nonomiya J, Pang J, et al. (2011). GDC-0980 is a novel class I PI3K/mTOR kinase inhibitor with robust activity in cancer models driven by the PI3K pathway. *Mol Cancer Ther* **10**, 2426–2436.

[30] Salphati L, Pang J, Plise EG, Lee LB, Olivero AG, Prior WW, Sampath D, Wong S, and Zhang X (2012). Preclinical assessment of the absorption and disposition of the phosphatidylinositol 3-kinase/mammalian target of rapamycin inhibitor GDC-0980 and prediction of its pharmacokinetics and efficacy in human. *Drug Metab Dispos* **40**, 1785–1796.

[31] Liang WC, Wu X, Peale FV, Lee CV, Meng YG, Gutierrez J, Fu L, Malik AK, Gerber HP, Ferrara N, et al. (2006). Cross-species vascular endothelial growth factor (VEGF)-blocking antibodies completely inhibit the growth of human tumor xenografts and measure the contribution of stromal VEGF. *J Biol Chem* **281**, 951–961.

[32] Tropres I, Grimault S, Vaeth A, Grillon E, Julien C, Payen JF, Lamalle L, and Decorps M (2001). Vessel size imaging. *Magn Reson Med* **45**, 397–408.

[33] Jensen JH and Chandra R (2000). MR imaging of microvasculature. *Magn Reson Med* **44**, 224–230.

[34] Tofts PS, Berkowitz B, and Schnall MD (1995). Quantitative analysis of dynamic Gd-DTPA enhancement in breast tumors using a permeability model. *Magn Reson Med* **33**, 564–568.

[35] O'Connor JP, Jackson A, Parker GJ, Roberts C, and Jayson GC (2012). Dynamic contrast-enhanced MRI in clinical trials of antivascular therapies. *Nat Rev Clin Oncol* **9**, 167–177.

[36] Wei K, Jayaweera AR, Firoozan S, Linka A, Skyba DM, and Kaul S (1998). Quantification of myocardial blood flow with ultrasound-induced destruction of microbubbles administered as a constant venous infusion. *Circulation* **97**, 473–483.

[37] Liu P, Cheng H, Roberts TM, and Zhao JJ (2009). Targeting the phosphoinositide 3-kinase pathway in cancer. *Nat Rev Drug Discov* **8**, 627–644.

[38] Bendell JC, Rodon J, Burris HA, de Jonge M, Verweij J, Birle D, Demanse D, De Buck SS, Ru QC, Peters M, et al. (2012). Phase I, dose-escalation study of BKM120, an oral pan-Class I PI3K inhibitor, in patients with advanced solid tumors. *J Clin Oncol* **30**, 282–290.

[39] Busaidy NL, Farooki A, Dowlati A, Perentesis JP, Dancey JE, Doyle LA, Brell JM, and Siu LL (2012). Management of metabolic effects associated with anticancer agents targeting the PI3K-Akt-mTOR pathway. *J Clin Oncol* **30**, 2919–2928.

[40] Nakatsu MN, Sainson RC, Aoto JN, Taylor KL, Aitkenhead M, Perez-del-Pulgar S, Carpenter PM, and Hughes CC (2003). Angiogenic sprouting and capillary lumen formation modeled by human umbilical vein endothelial cells (HUVEC) in fibrin gels: the role of fibroblasts and Angiopoietin-1. *Microvasc Res* **66**, 102–112.

[41] Gutierrez J, Konecny GE, Hong K, Burges A, Henry TD, Lambiase PD, Lee Wong W, and Meng YG (2008). A new ELISA for use in a 3-ELISA system to assess concentrations of VEGF splice variants and $VEGF_{110}$ in ovarian cancer tumors. *Clin Chem* **54**, 597–601.

[42] Carano RA, Ross AL, Ross J, Williams SP, Koeppen H, Schwall RH, and Van Bruggen N (2004). Quantification of tumor tissue populations by multispectral analysis. *Magn Reson Med* **51**, 542–551.

[43] Bates DO, Lodwick D, and Williams B (1999). Vascular endothelial growth factor and microvascular permeability. *Microcirculation* **6**, 83–96.

[44] Qayum N, Im J, Stratford MR, Bernhard EJ, McKenna WG, and Muschel RJ (2012). Modulation of the tumor microvasculature by phosphoinositide-3 kinase inhibition increases doxorubicin delivery *in vivo*. *Clin Cancer Res* **18**, 161–169.

[45] Kelloff GJ, Hoffman JM, Johnson B, Scher HI, Siegel BA, Cheng EY, Cheson BD, O'Shaughnessy J, Guyton KZ, Mankoff DA, et al. (2005). Progress and promise of FDG-PET imaging for cancer patient management and oncologic drug development. *Clin Cancer Res* **11**, 2785–2808.

[46] Lamuraglia M, Escudier B, Chami L, Schwartz B, Leclere J, Roche A, and Lassau N (2006). To predict progression-free survival and overall survival in metastatic renal cancer treated with sorafenib: pilot study using dynamic contrast-enhanced Doppler ultrasound. *Eur J Cancer* **42**, 2472–2479.

[47] Batchelor TT, Sorensen AG, di Tomaso E, Zhang WT, Duda DG, Cohen KS, Kozak KR, Cahill DP, Chen PJ, Zhu M, et al. (2007). AZD2171, a pan-VEGF receptor tyrosine kinase inhibitor, normalizes tumor vasculature and alleviates edema in glioblastoma patients. *Cancer Cell* **11**, 83–95.

[48] Genentech (2009). *A Study Evaluating GDC-0980 Administered Once Weekly in Patients with Refractory Solid Tumors or Non-Hodgkin's Lymphoma.* NCT00854126, The United States National Institutes of Health. Available at: http://clinicaltrials.gov/.

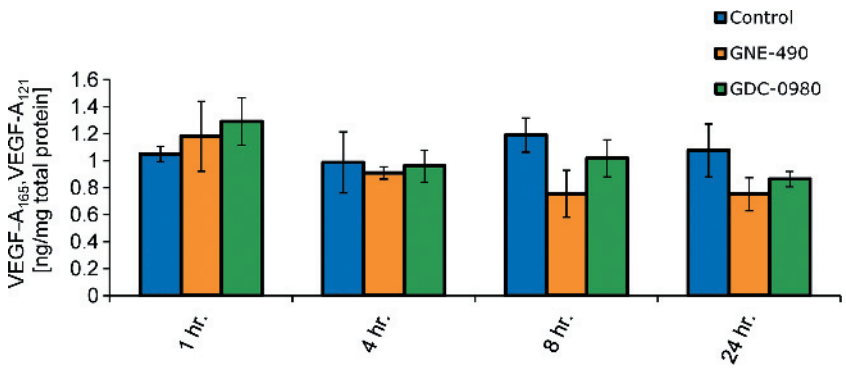

Figure W1. Tumor VEGF-A levels are not reduced after treatment with class I PI3K selective (GNE-490) or dual PI3K/mTOR (GDC-0980) inhibitors *in vivo*. HM-7 tumor–bearing mice ($n = 4$/group) were treated with a single oral dose of vehicle, GNE-490 (30 mg/kg), or GDC-0980 (10 mg/kg). Tumors from each group were harvested 1, 4, 8, and 24 hours post-dose and analyzed for expression of VEGF-A isoforms 121 and 165 by ELISA as described in Materials and Methods section.